Bone 127 (2019) 577–591

Contents lists available at ScienceDirect

Bone

journal homepage: www.elsevier.com/locate/bone

Full Length Article

Transcriptional profiling of intramembranous and endochondral ossification after fracture in mice☆,☆☆

Brandon A. Coates[a,b,*], Jennifer A. McKenzie[a], Evan G. Buettmann[a,b,1], Xiaochen Liu[a,2], Paul M. Gontarz[c], Bo Zhang[c], Matthew J. Silva[a,b]

[a] Department of Orthopaedic Surgery, Washington University in St. Louis, MO, United States of America
[b] Department of Biomedical Engineering, Washington University in St. Louis, MO, United States of America
[c] Department of Developmental Biology, Washington University in St. Louis, MO, United States of America

ARTICLE INFO

Keywords:
Fracture repair
Transcriptome
Animal models
Bone

ABSTRACT

Bone fracture repair represents an important clinical challenge with nearly 1 million non-union fractures occurring annually in the U.S. Gene expression differs between non-union and healthy repair, suggesting there is a pattern of gene expression that is indicative of optimal repair. Despite this, the gene expression profile of fracture repair remains incompletely understood. In this work, we used RNA-seq of two well-established murine fracture models to describe gene expression of intramembranous and endochondral bone formation. We used top differentially expressed genes, enriched gene ontology terms and pathways, callus cellular phenotyping, and histology to describe and contrast these bone formation processes across time. Intramembranous repair, as modeled by ulnar stress fracture, and endochondral repair, as modeled by femur full fracture, exhibited vastly different transcriptional profiles throughout repair. Stress fracture healing had enriched differentially expressed genes associated with bone repair and osteoblasts, highlighting the strong osteogenic repair process of this model. Interestingly, the PI3K-Akt signaling pathway was one of only a few pathways uniquely enriched in stress fracture repair. Full fracture repair involved a higher level of inflammatory and immune cell related genes than did stress fracture repair. Full fracture repair also differed from stress fracture in a robust downregulation of ion channel genes following injury, the role of which in fracture repair is unclear. This study offers a broad description of gene expression in intramembranous and endochondral ossification across several time points throughout repair and suggests several potentially intriguing genes, pathways, and cells whose role in fracture repair requires further study.

1. Introduction

Skeletal fractures are an important clinical problem. About 16 million fractures occur annually in the U.S. – roughly one every two seconds [1]. Over the next decade, the national economic burden of fractures is estimated at $25 billion. Bones have a strong capacity for self-repair and, with proper intervention, most fractures will heal without major complications. Importantly though, about 5 to 10% of fracture patients will not heal adequately – suffering from either delayed- or non-union healing [2]. Delayed and non-union fractures are painful, costly, and require additional surgical interventions. Although many comorbidities are associated with nonunions, their molecular pathogenesis is unclear, thus representing an important target for research [3].

Bones fracture in several ways, depending on the mechanical cause of injury. Two broad categories, stress fractures and full fractures, are the focus of this work. Stress fractures are defined by a crack which is partially propagated, non-displaced, and unicortical [4,5]. Stress fractures are caused by repetitive overuse that leads to bone fatigue damage [6,7]. Alternatively, full fractures occur by complete propagation of one or more cracks across the bone cortices, resulting in a displaced fracture [8]. Full fractures are typically caused by a sudden overload of the

☆ Grant supporters: NIAMS (R01 AR050211, P30 AR057235, P30 AR074992), NIBIB (T32 EB018266).
☆☆ Funding supporters played no role in study design, collection, analysis and interpretation of data, or writing of this report.
* Corresponding author at: BJCIH 11th Floor, RM 11511, Campus Box 8233, Orthopaedic Surgery, United States of America.
E-mail address: bcoates@wustl.edu (B.A. Coates).
[1] Present affiliation: Department of Biomedical Engineering, Virginia Commonwealth University, United States of America.
[2] Present affiliation: Department of Radiology, University of Toledo Medical Center, United States of America.

https://doi.org/10.1016/j.bone.2019.07.022
Received 11 April 2019; Received in revised form 27 June 2019; Accepted 18 July 2019
Available online 29 July 2019

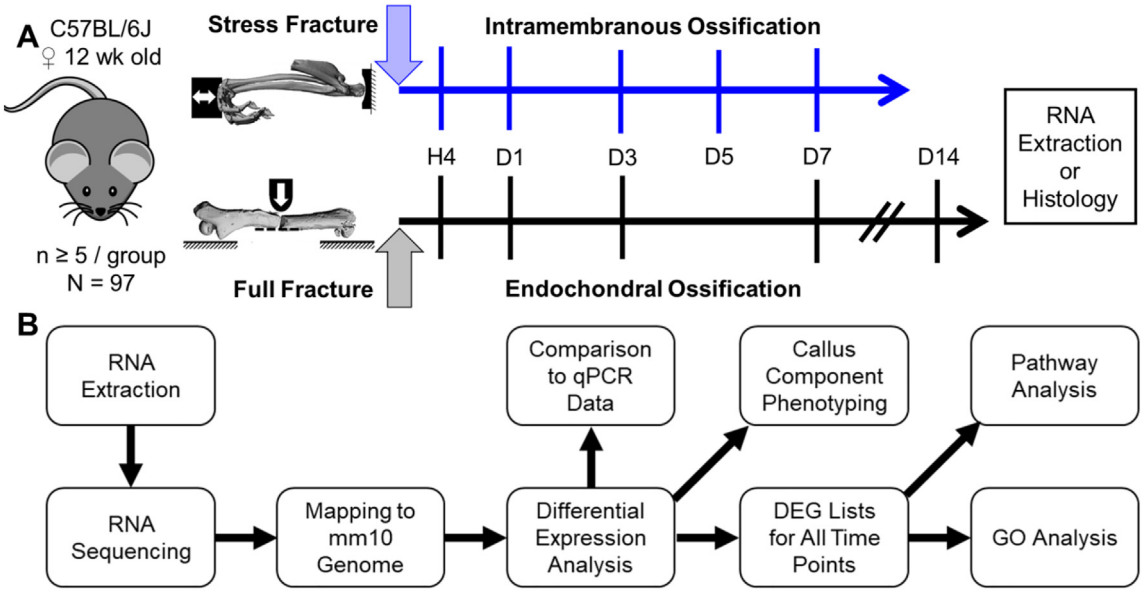

Fig. 1. Experimental overview of fracture models, time points, and RNA-seq pipeline. (A) 97 female C57BL/6J mice were injured with stress or full fracture, sacrificed at 4 h, 1, 3, 5, 7, or 14 days post-injury, and processed for RNA-seq or histology. (B) RNA-seq analysis began with RNA extraction from pulverized bone tissue. RNA was sequenced and reads were mapped to mm10 genome. Differential expression analysis was performed to create lists of differentially expressed genes (DEGs) for each time point. Comparison to previously generated qPCR data of stress and full fracture callus was used to validate RNA-seq data. Callus component analysis using transcriptional profiling of callus cells was performed at each time point. Pathway analysis and GO annotation were performed on the DEG lists of each time point.

bone, as experienced in trauma. These different injuries trigger distinct repair cascades.

Stress fractures heal by intramembranous ossification, the direct formation of a bone callus without a cartilaginous intermediary [9]. Full fracture heals primarily through endochondral ossification, which features an intermediary cartilaginous callus [10] that is then replaced by bone, with some intramembranous ossification occurring at the stable margins of the fracture callus. The stability of the injury site and the displacement caused by the injury determine which bone formation mechanism occurs [11]. Intramembranous ossification is favored by stable injuries with little displacement and endochondral ossification is preferential when injuries are unstable and displaced. The distinct processes for intramembranous and endochondral bone formation are well documented – and transcriptomic analysis of each has individually been reported. Several studies have used microarray technology to assay gene expression in models of endochondral ossification in mouse [12–14], rats [15], and humans [16], and additional work has been performed using RNA-seq in mouse [17]. These works describe the complex transcriptional response following full fracture, which involves, inflammatory, angiogenic, chondrogenic, and osteogenic processes. There are few reports of gene expression in intramembranous ossification, with one report using microarray to study stress fracture healing in rat [18], which described strong expression of inflammatory, angiogenic, and osteogenic genes.

While these studies were illuminating, a more direct comparison of the gene expression profiles of intramembranous and endochondral ossification might provide additional insight. For example, while both processes involve inflammation, the relative scale of the inflammatory response is likely to be less after stress fracture than full fracture. Furthermore, sampling from several time points following injury will provide information on how gene transcription changes throughout repair. A comparison of intramembranous and endochondral ossification spanning several time points across the repair window, using contemporary RNA-seq analysis, would address these knowledge gaps and shed light on similarities and differences between these two processes. Studies have shown that transcriptional differences exist between successful and non-union bone fracture repair [16] as well as young mice and slowly healing geriatric mice [12]. However, gene expression of poor healing is difficult to utilize if normal healing is incompletely understood. Therefore, a more comprehensive understanding of the transcription of endochondral and intramembranous ossification could better inform the treatment of delayed- and non-union fractures.

The goal of this work is to provide a detailed description of the temporal transcriptional response occurring in the fracture repair processes of intramembranous and endochondral ossification. We used two well-established murine fracture models and RNA sequencing to assay gene expression at five time points following stress fracture and full fracture. We hypothesized that endochondral repair would feature a greater number of differentially expressed genes than intramembranous repair, and that many of the genes unique to full fracture would be related to inflammation and chondrogenesis. Furthermore, we hypothesized that this analysis would reveal novel transcriptional differences between these two healing modalities.

2. Materials and methods

2.1. Mice

Within an IACUC approved protocol, a total of 97 female C57BL/6J wild-type mice (Jackson Labs) were obtained at 9 weeks old and were aged to 12 weeks old for experimental use. We chose a single sex to limit the scope of the study, and selected females because women have higher rates of fracture [19,20]. Mice were kept on a 12:12 light/dark cycle and were fed chow ad libitum. A group of 47 mice were subjected to unilateral ulnar stress fracture and were randomly assigned to post-fracture time points of 4 h, 1, 3, 5, or 7 days for either RNA extraction ($N = 25$) or histological processing ($N = 22$) (Fig. 1A). Additionally, a set of 50 mice were subjected to unilateral full femur fracture and were randomly assigned to post-fracture time points of 4 h, 1, 3, 7, or 14 days for either RNA extraction ($N = 35$) or histology processing ($N = 15$) (Fig. 1A). We selected time points based on historical data to survey the various important phases of the early fracture repair response (i.e. inflammation, angiogenesis, chondrogenesis, and early osteogenesis).

Differences in the later time points reflect the relatively longer time to peak osteogenesis in full versus stress fracture repair. All animals were healthy at time of injury and body weight was consistent between groups (mean body weight = 20.8 ± 1.3 g). Mice were euthanized by CO_2 asphyxia at the assigned post-injury time point.

2.2. Stress fracture

We used ulnar stress fractures to study intramembranous ossification. The murine forelimb fatigue model used to create stress fractures was described in detail in previous reports [21,22]. Briefly, mice were anesthetized with 1–3% isoflurane and the right forelimb was positioned between two fixtures on a material testing machine (Instron Dynamite). Calibration mice were loaded with a monotonic displacement ramp to determine ultimate force of the forelimb and with cyclic compression to determine fracture displacement. Experimental mice were loaded using force-controlled cyclic compression to a peak of 3.0 N (75% of mean ultimate force, 2 Hz) applied to the forelimb until an increase in total displacement of 0.5 mm (50% of mean fracture displacement) was achieved. The average number of cycles applied was 5383 (range: 105–18,627). Time zero for the stress fracture was considered to be the time of the final loading cycle, as the crack growth mostly occurs in the last few cycles of loading. The left ulna served as a non-injured contralateral control. Following loading, the mouse was administered buprenorphine (0.1 mg/kg, s.c.) for analgesia and returned to the cage with unrestricted activity until time of sacrifice. Mice returned to subjectively normal activity levels within minutes of being returned to their cage.

2.3. Full fracture

We used femur full fractures to study endochondral ossification. The femur fracture procedure was described in detail in previous reports [23]. In brief, mice were anesthetized with 1–3% isoflurane, and slow release buprenorphine (1 mg/kg, s.c.) was administered for pain management. The right femur was exposed through a small incision and notched with a scalpel to pre-dispose the mid-diaphysis to fracture. The right hind limb was then secured in a three-point bending fixture on a material testing machine (Instron Dynamite) and a monotonic displacement ramp (30 mm/s) was applied to produce a transverse fracture in the mid-diaphysis of the femur. A 24G pin was inserted into the intramedullary space to provide mechanical stability and the incision was closed. Fracture location and pin placement were confirmed by X-ray radiography (Faxitron UltraFocus). Mice were then returned to unrestricted cage activity and reached relatively normal activity levels within a few hours of the procedure. Generation of fractures had good reproducibility with consistent tissue damage, actuator displacement, stability of the fracture, and lack of comminution. The left femur served as a non-fractured contralateral control. Radiographs were again taken at time of sacrifice to reconfirm intramedullary pin placement. Mice were excluded from analysis if fracture occurred outside the mid-diaphysis ($n = 5$) or if the stabilization pin had slipped from the intramedullary space by time of sacrifice ($n = 1$).

2.4. RNA extraction and sequencing

For stress fracture, a 5 mm section of the ulna was removed surrounding the injury site. Soft tissue was removed, the sample was flash frozen in liquid nitrogen, and stored at −80 °C until RNA extraction. The left ulna was similarly processed to serve as a control. For full fracture, a 7 mm section of the femur was removed surrounding the injury site. Soft tissue was removed and bone marrow was spun out using a centrifuge. The sample was flash frozen in liquid nitrogen and stored at −80 °C until RNA extraction. The left femur was similarly processed to serve as a control.

Frozen bone samples were pulverized (Braun Mikrodismembrator), dissolved into TRIzol (Invitrogen), and stored at −80 °C. Later, the TRIzol-sample solution was thawed and processed using an RNA clean-up and concentration kit (Norgen Biotek) (Fig. 1B). RNA concentration was measured (Thermo Scientific Nanodrop ONE) and quality was evaluated (Agilent Technologies Bioanalyzer 2100). Only samples with RINs > 6.5, representing acceptable quality, were used in sequencing; samples not meeting this criterion were excluded ($n = 4$).

A total of 70 samples were subjected to RNA-seq (Fig. 1B). For each fracture type, there were 25 fracture samples ($n = 5$/time point) and 10 control samples ($n = 2$/time point). Total RNA was depleted of rRNA (Illumina, Ribo-Zero rRNA Removal Kit) and RNA-seq (Illumina HiSeq 3000) was performed at 1 × 50 bp on 1 μg of RNA by the Washington University Genome Technology Access Center. The RNA-seq reads were aligned to the mm10 mouse genome (STAR version 2.4.2a). Gene counts were derived from the number of uniquely aligned unambiguous reads (Subread:featureCount, version 1.4.6) and annotated (GENCODE v9). Only non-redundant uniquely aligned reads were used to estimate the expression level of genes. All gene-level transcript counts were then normalized for library size (R/Bioconductor DEseq2). Lowly expressed genes (CPM < 1) in all the samples at any time points were filtered out, and resulted in 17,240 genes for down-stream analysis. To check for outlier samples a correlation analysis was performed (cutoff of $r > 0.85$). In stress fracture, three samples (one each from control, day 1, and day 7) were flagged as outliers and removed from further analysis. In full fracture, all samples passed this inspection. Differential expression analysis was performed separately for each injury mode and each time point as a comparison of injured samples vs. pooled control samples, with a threshold for differentially expressed genes (DEGs) set as fold-change (FC, Injured/Control) > 2 and Benjamini-Hochberg adjusted p-value < 0.05. Additional characterization was performed by a principle component analysis on stress fracture and full fracture samples separately. For each sample, the reads per kilobase of transcript per million mapped reads (RPKM) values for all 17,240 genes in the data set were used as inputs.

2.5. Validation of RNA-seq data

In order to validate RNA-seq gene expression, we made comparisons to qPCR data previously generated in our lab using similar fracture models on control mice of similar age, size, and background. Fold change (FC) values for full fracture at days 7 and 14 post-injury, and stress fracture at days 1, 3, and 7 post-injury were correlated to FC values previously reported for 49 transcripts resulting in 94 comparisons as some transcripts were in multiple time points (Supplementary Table 1) [21–23]. Additionally, we performed qPCR for select genes on remaining RNA from full fracture samples. Collagen Type 1a1 (*Col1a1*), Aggrecan (*Acan*), and Potassium Voltage-Gated Channel Subfamily J Member 5 (*Kcnj5*) were chosen in order to sample genes from various processes with differing expression profiles. cDNA was produced (Biorad iScript) from 500 ng of RNA for all full fracture samples from days 1, 3, 7 and 14 and corresponding contralateral femurs. qRT-PCR was performed (Applied Biosystems StepOnePlus) using primers (IDT PrimeTime) for *Col1a1* (Mm.PT.58.7562513), *Acan* (Mm.PT.58.23585796), and *Kcnj5* (Mm.PT.58.6016350) and reference genes TATA Binding Protein (*Tbp*, Mm.PT.58.42394711) and Importin 8 (*Ipo8*, Mm.PT.39a.22214844). Expression was normalized to reference genes and fold changes were determined by ΔΔCT method comparing to contralateral limb.

2.6. Gene ontology and pathway analyses

For gene ontology analysis, each of the ten DEG lists (2 injury types × 5 time points) was input into the Database for Annotation, Visualization and Integrated Discovery (DAVID) system as a gene list [24,25]. Annotations were limited to *Mus musculus*. Biological process gene ontology (GO) terms and enriched pathways from the Kyoto

Encyclopedia of Genes and Genomes (KEGG) database were obtained for each list and filtered to remove non-significant terms (Bonferroni $p < 0.05$).

2.7. Callus component phenotyping

To identify various populations of cells in the callus following stress or full fracture, we followed an approach described by Angelova et al. in the immunophenotyping of tumor biopsies [26]. Briefly, they used RNA-seq of bulk tumor biopsies and compared the gene expression against curated lists comprised of genes specific to certain immune cell types. By comparing the gene expression of curated lists, a census of immune cells residing in the tumor can be inferred. In a similar manner, we used RNA-seq of fracture callus tissue, in combination with curated gene lists, to infer the cellular populations present at various stages of stress and full fracture repair. Gene lists were compiled from literature reviews for neutrophils, macrophages, monocytes, T cells, and B cells [26]; as well as osteoblasts [27,28], osteoclasts [29–33], endothelial cells [34,35], and chondrocytes [36–39] (Supplementary Table 2). We then examined the fold change of these genes across time following stress and full fracture as an estimate of the abundance of each cell type within the callus.

2.8. Histology

Following sacrifice, injured limbs from stress fracture ($n = 22$) and full fracture ($n = 15$) were harvested and placed in 10% neutral buffered formalin for 24 h. Tissue was decalcified for 14 days using 14% EDTA, embedded in paraffin, and longitudinal cuts were made for histological observation and immunohistochemistry (IHC) processing. Histological sections of each time point were stained with hematoxylin and eosin (H&E) to show the progression of healing in each fracture type at each time point in the study (Fig. 2).

Antibodies for Gr-1 (Bio-Rad MCA2387T, 1:500 dilution), F4/80 (Bio-Rad, MCA497RT 1:500 dilution), and CD45 (BD Pharmingen 550539, 1:500 dilution) were used with an ImmPRESS Reagent Anti-Rat IgG (VectaShield MP-7404) kit to stain for infiltration of neutrophils, macrophages, and leukocytes, respectively. An antibody for p-Akt T308 (Cell Signaling #2965) was used with a goat anti-rabbit/HRP secondary antibody (Dako P0448) in order to stain for activation of the PI3K-Akt signaling pathway. Sections were counterstained with hematoxylin (Modified Mayer's, Electron Microscopy Services). Following staining, slides were imaged using a Nanozoomer slide scanner (Hamamatsu) at 20× magnification.

3. Results

3.1. RNA-seq data correlates to previous fracture gene expression data

Plots of principle components 1, 2, and 3 for all samples in stress fracture (Fig. 3A) and full fracture (Fig. 3B) were compiled. Samples clustered by time point and adjacent time points were closest together on the plots. Additionally, gene expression values from RNA-seq and previously published qPCR data were strongly correlated ($r = 0.75$) and clustered around the identity line (Fig. 3C). Fold changes from qPCR performed on remaining RNA from full fracture samples also closely corresponded to those from the RNA-seq analysis (Fig. 3C). These data supported the accuracy of RNA-seq to describe post-fracture transcriptional changes, affirmed the integrity of these samples, and confirmed the validity of pooling controls and samples within time points.

3.2. Dramatic transcription changes during fracture repair

Overall, there were approximately 17,240 genes with high enough expression to be included in DEG analysis. Of these, 7383 were differentially expressed genes (DEGs) in at least one time point and fracture type. Stress fracture repair had few early responding genes with only 87 DEGs at 4 h and 124 DEGs at day 1 following injury (Fig. 4A). This number increased to 1099 DEGs by day 3 and peaked with 1434 DEGs at 5 days post-injury. From 5 to 7 days post injury, the number of DEGs declined. On the other hand, full fracture resulted in many early changes in gene expression, with over 2000 DEGs at 4 h post-injury (Fig. 4B). The number of DEGs remained high across all time points and peaked at 4474 DEGs at 7 days post-injury. After full fracture, more genes were downregulated than upregulated across all time points. In contrast, more genes were upregulated at all stress fracture repair time points.

Gene expression varied greatly across time, with few genes differentially expressed across all time points. The largest DEG subsets were those unique to only one time point or those shared by consecutive time points – especially the later ones (Fig. 4C & D). For example, in stress fracture the largest DEG subset is the one shared between days 3, 5, and 7 post-fracture (571 DEGs). The numbers of DEGs shared between any two time points further highlights that the greatest number of shared DEGs occurs between adjacent time points (Supplementary Fig. 1).

Across all time points, 1469 DEGs were shared between stress fracture and full fracture, while 5497 DEGs were unique to full fracture, and 210 were unique to stress fracture repair (Supplementary Fig. 2A). A similar trend was observed for each time point comparison, with the largest number of DEGs unique to full fracture, a smaller subset shared between the two injuries, and the fewest DEGs unique to stress fracture. Each subgroup was analyzed for enriched GO terms and pathways (Supplementary Fig. 2B).

3.3. Stronger expression changes in full fracture repair

The top ten up- and downregulated DEGs at every time point were compiled (Table 1). In stress fracture, genes involved in inflammation and matrix degradation were upregulated at early time points. Among these were Prostaglandin-Endoperoxide Synthase 2 (*Ptgs2*), Suppressor of Cytokine Signaling 3 (*Socs3*), and metalloproteinases *Mmp3*, *Adamts4*, and *Timp1*. Ras Related Glycolysis Inhibitor and Calcium Channel Regulator (*Rrad*) was among the top upregulated genes at H4 and D1 post-stress fracture. *Rrad* is involved in bone homeostasis and knockout of *Rrad* leads to osteopenia [40]. Pannexin 3 (*Panx3*) and C1q and TNF Related 3 (*C1qtnf3*) are the top most upregulated DEGs at days 3, 5, and 7 post-stress fracture. Both *Panx3* and *C1qtnf3* are expressed in osteoblasts [41]. *Panx3* is a putative Runx2 target [42] and is important in osteoblast differentiation and regulation of the Wnt/β-catenin pathway [43]. In the context of bone, *C1qtnf3* is less understood, but may also influence osteoblast differentiation [44,45]. The greatest FC values occurred at D5, which is also the time point with the largest number of DEGs. Interestingly, genes associated with chondrogenesis (*Col9a1/2/3*, *Col2a1*, *Acan*) are highly upregulated despite the relatively small amount of cartilage tissue in the stress fracture callus [46]. However, these may not necessarily be due to chondrocytes, as osteoblasts also express these transcripts [41]. Appearing among the early downregulated genes are Dickkopf WNT Signaling Pathway Inhibitor 1 (*Dkk1*) and Sclerostin (*Sost*) – both known inhibitors of bone formation [47,48].

In full fracture, inflammatory genes exhibited the largest fold changes at the early time points. Among these were the C-X-C Motif Chemokine Ligands 1, 2, 3 and 5 (*Cxcl1*, *Cxcl2*, *Cxcl3*, and *Cxcl5*), which are attractants of immune cells and endothelial cells [49–51], as well as *IL-6*, *IL-11*, and *Ptgs2*, all important chemokines in bone repair [52–56]. Arginase 1 (*Arg1*), an essential metabolite in collagen synthesis and wound repair, was also highly upregulated at several time points [57]. Like stress fracture, the largest FC values occurred at the penultimate time point (day 7), when there was a large upregulation of chondrocyte related genes (*Col9a1/2/3*, *Col10a1*, *Matn1/2*); the peak fold changes in chondrocyte related genes were an order of magnitude greater in full fracture than stress fracture (e.g., *Col9a1*: FC = 440, D7 full fracture vs.

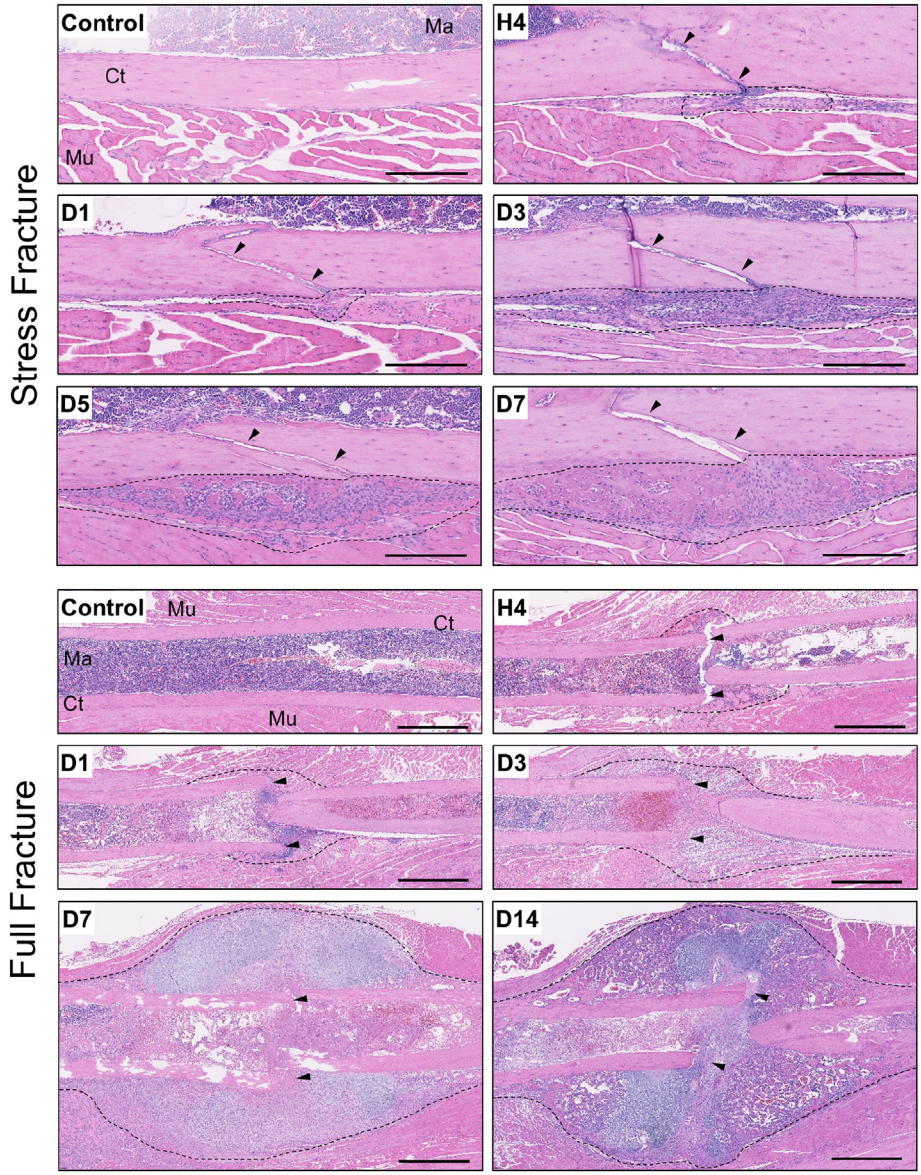

Fig. 2. Progression of healing of stress fracture and full fracture over time. H&E staining of paraffin sections of stress fracture or full fracture callus. Scale bars represent 250 μm for stress fracture images and 1 mm for full fracture images. Ct = Cortical Bone, Ma = Marrow, Mu = Muscle, ▲ = stress fracture or full fracture line, dotted line = callus.

FC = 35, D5 stress fracture). Among the most downregulated genes in full fracture repair are those related to myosin (*Myl2*, *Myl3*, *Myh7*, and *Mylk4*) and genes from the immunoglobin superfamily (*Ly6g6f*, *G6b*, and *Gp6*).

3.4. GO term analysis

115 GO terms were significantly enriched in at least one time point and fracture type (Fig. 5A). Of these, 17 GO terms were shared between both injuries, while 16 terms were unique to stress fracture and 82 were unique to full fracture (Fig. 5B). Enriched GO terms were compared across time points and injury type (Fig. 5C). Early time points showed no GO terms that were unique to stress fracture. In contrast, at day 3 through day 7 several terms related to osteogenesis were unique to stress fracture repair, such as "*collagen fibril organization*", "*osteoblast differentiation*", "*bone development*", "*bone mineralization*", and "*negative regulation of Wnt signaling*".

GO terms shared between stress and full fracture were few at early time points and included "*response to cytokine*" and "*positive regulation of transcription from Polr promoter*" at 4 h, and "*positive regulation of cell migration*" at day 1 post injury. Later time points had shared terms such as "*angiogenesis*", "*extracellular matrix organization*", "*ossification*", and "*cartilage development*".

Terms unique to full fracture repair included those related to inflammation ("inflammatory response", "chemokine-mediated signaling pathway", "cellular response to IL-1", and "innate immune response"), metabolism ("oxidation-reduction process", "glucose metabolic process", and "response to hypoxia"), and ion transport ("potassium ion transmembrane transport", "cellular calcium ion homeostasis", and "ion transport").

3.5. Pathway analysis

60 pathways were significantly enriched in at least one time point and fracture type (Fig. 6A). Of these pathways, 12 were enriched in both stress and full fracture, while 3 were uniquely enriched in stress fracture, and 45 were uniquely enriched in full fracture (Fig. 6B). Of the three pathways unique to stress fracture, only the "*PI3K-Akt signaling*

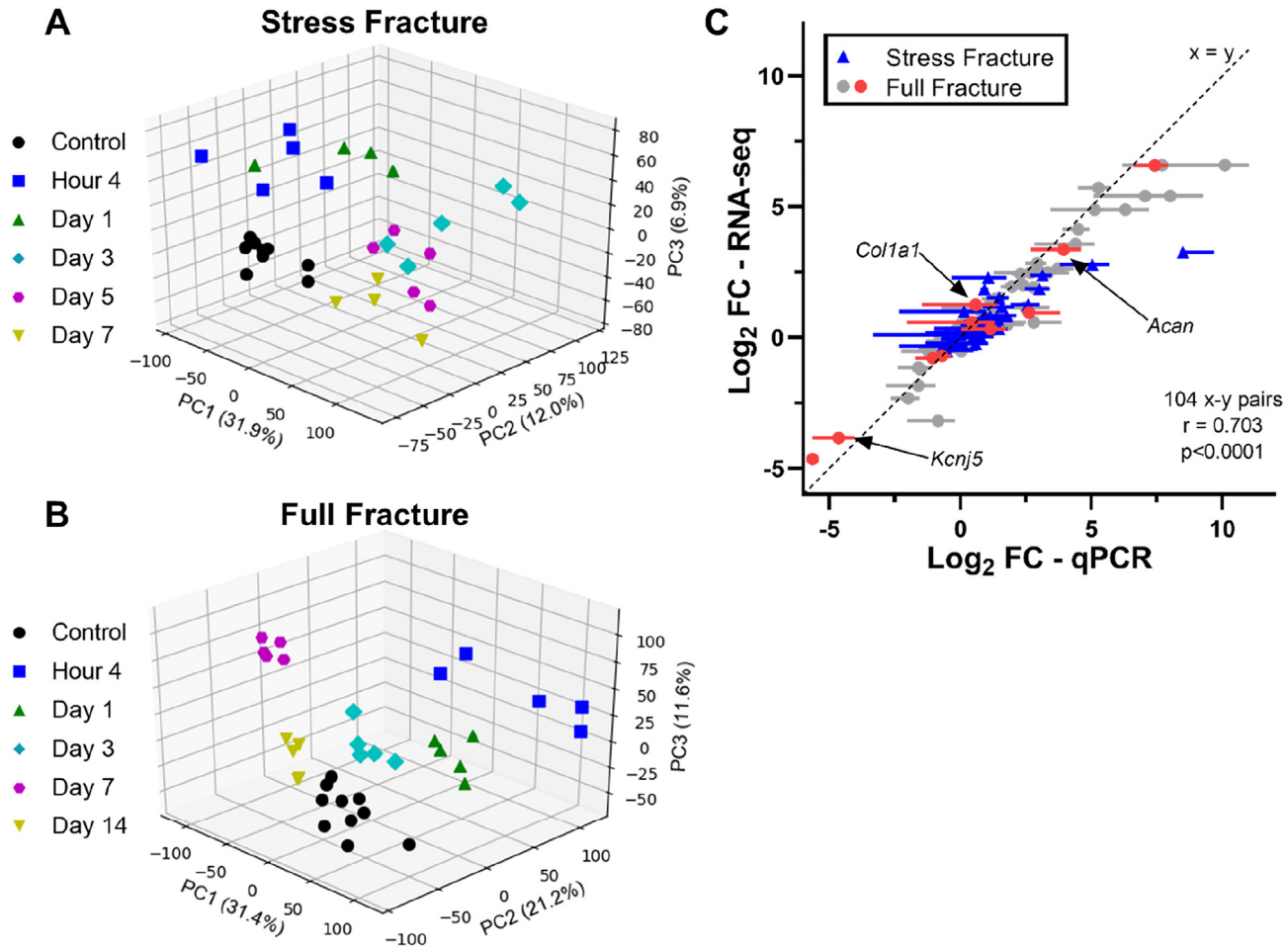

Fig. 3. Validation of RNA-seq data. Principle component analysis (PCA) of all samples in stress fracture (A) and full fracture (B). Samples within time points cluster together and time point clusters were grouped closely with adjacent time points. (C) Correlation of RNA-seq data with analogous qPCR data from previous published reports of stress fracture (blue triangle) and full fracture (grey circle) and concurrent qPCR of full fracture samples (red circle). Log2 fold change (injured vs. control) from RNA-seq was plotted versus log2FC from qPCR (± standard deviation). Data is plotted from multiple time points for each injury. A linear regression confirmed strong correlation between RNA-seq and qPCR data. Genes from published reports are detailed in Supplementary Table 1. Select genes from concurrent qPCR are labeled with arrows. (For interpretation of the references to color in this figure legend, the reader is referred to the web version of this article.)

pathway" was enriched at multiple time points (Fig. 6C). Pathways that were shared between stress and full fracture repair include those related to the immune system and diseases ("*TNF signaling*", "*cytokine-cytokine receptor signaling*", "*systemic lupus erythematosus*", and "*malaria*") as well as pathways like "*ECM-receptor interactions*", "*focal adhesions*", and "*arginine and proline metabolism*". Pathways uniquely enriched in full fracture repair include those related to immune processes ("*Rheumatoid arthritis*", "*NFκB signaling*", "*toll-like receptor signaling*"), metabolism ("*glycolysis/gluconeogenesis*", "*insulin resistance*", "*galactose metabolism*") and cardiac muscle ("*hypertrophic cardiomyopathy*", "*cardiac muscle contraction*", "*calcium signaling*").

3.6. Callus component phenotyping

To estimate the abundance of cell types within fracture callus throughout repair, the fold change of genes on curated lists (Supplementary Table 2) were compiled for each time point and fracture type (Fig. 7). Neutrophil related genes were strongly upregulated at early time points (hour 4, day 1) following full fracture (Fig. 7A), and slightly increased after stress fracture (hour 4). At later time points, most neutrophil-related genes were downregulated (days 5, 7, and 14). Macrophage related genes displayed a mix of up- and downregulation within time points and thus no clear pattern was evident (Fig. 7B). Monocyte related genes were upregulated at multiple time points in both stress and full fracture, most strongly at early time points (hour 4 and day 1) after full fracture (Fig. 7C). T cell associated genes were upregulated early post stress fracture (hour 4) and full fracture (hour 4 and day 1), but suppressed at later time points (days 5, 7, and 14) (Fig. 7D). B cell related genes were mostly suppressed after stress fracture (days 1–7) and full fracture (days 3–14) (Fig. 7E). Osteoblast related genes were strongly expressed after stress fracture (days 3, 5, and 7) and to a slightly lesser extent following full fracture (days 3, 7, and 14) (Fig. 7F); these genes were down early (hour 4) post-full fracture. Osteoclast related genes did not show strong signal either up or down except for slight upregulation at the final time point of each injury (Fig. 7G). Endothelial cell related genes showed modest increases by later time points in both models (Fig. 7H). Chondrocyte related genes showed upregulation in both models at later time points (days 5, 7, and 14) (Fig. 7I).

3.7. IHC of fracture callus

Antibodies for Gr-1, F4/80, and CD45 were used to stain fracture callus to assess the presence of immune cells. Gr-1, a marker of neutrophils, was abundantly expressed in marrow in the contralateral control, but not in cortical bone, endosteum, or periosteum. At early post-injury time points (hour 4 - day 3) Gr-1 expressing cells were adjacent to the injury site in both stress and full fracture (Fig. 8). This

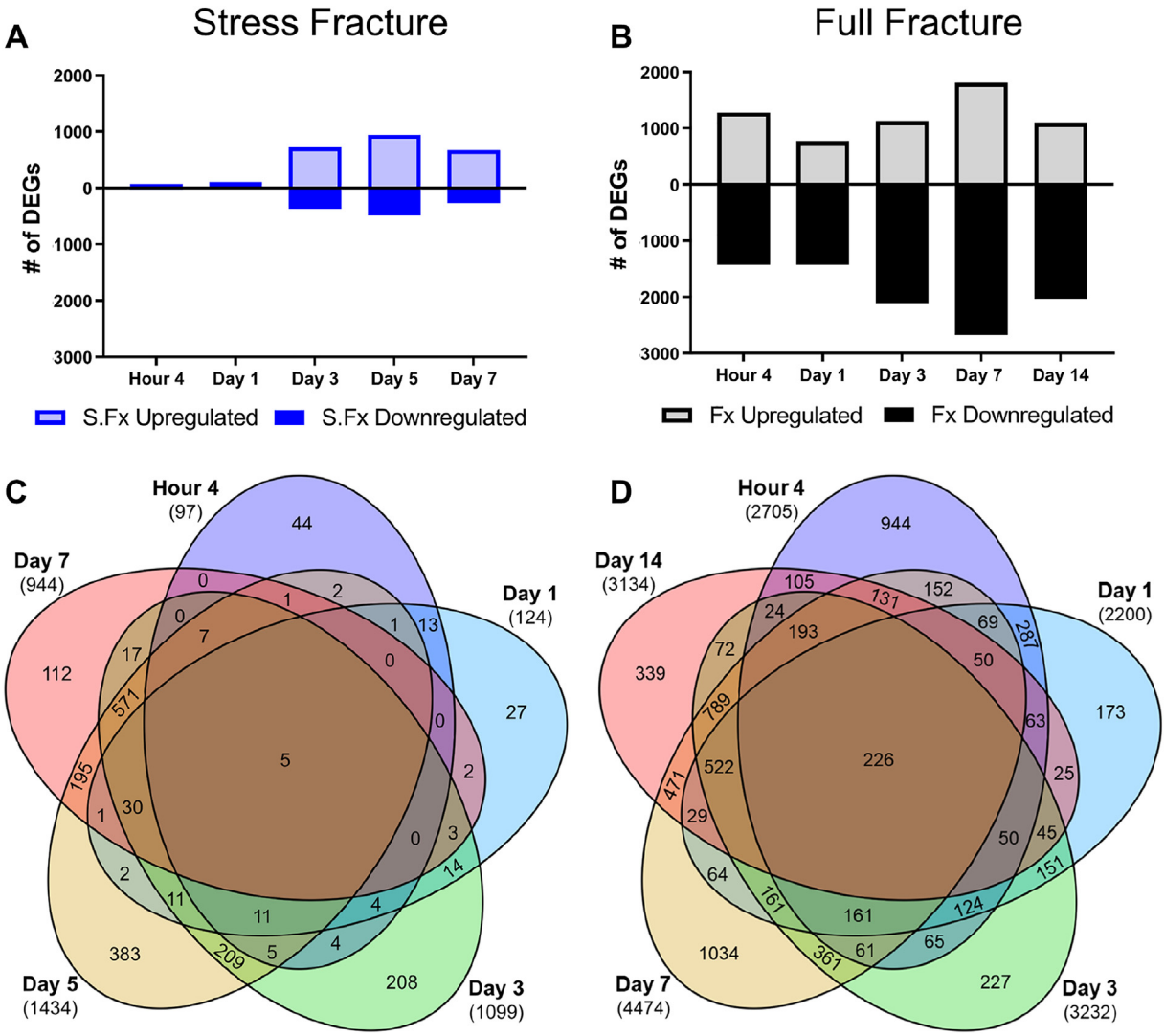

Fig. 4. DEG trends across time. Total number of DEGs at each time point are shown for stress fracture (A) and full fracture (B). Following stress fracture (S.Fx), few DEGs occurred early, but DEGs reached robust levels at later time points and peaked at day 5. Following full fracture (Fx), DEGs were immediately expressed at high levels that persisted through our experimental window, and peaked at day 7. Comparisons of the overlap of DEGs at each time point for stress fracture (C) and full fracture (D) are shown in 5-way Venn diagrams. Total number of DEGs at each time point are shown in parentheses. The largest lists were those unique to one time point or shared between adjacent time points.

signal was diminished at later time points (days 5, 7 and 14) - consistent with the callus component phenotyping analysis and suggesting a reduced role for neutrophils after the early injury response. Staining for F4/80, a marker for macrophages, showed strong signal in the bone marrow of control ulna and femur, but not in cortical bone, endosteum, or periosteum. Stress fracture repair did not lead to robust F4/80 staining at any time point, with only modest local staining at hour 4 post-injury; this is consistent with the lack of a strong macrophage signal from callus component phenotyping analysis. By contrast, in full fracture, F4/80 staining was present in callus at all time points with the most robust staining at D3 post-injury. CD45, a general marker of leukocytes, was most abundant at 1 and 3 days post stress fracture. In full fracture, CD45 showed robust staining at early time points (hour 4 – day 3) and was reduced by day 7 and 14. In summary, neutrophils abound in early callus of both stress and full fracture while macrophages appear to be more abundant in full fracture callus than stress fracture.

To confirm that PI3K-Akt signaling was active in stress fracture repair, we performed IHC staining for p-Akt T308. Little staining for p-Akt was present in contralateral bone or at day 1 after injury (Supplementary Fig. 3). By days 3, 5, and 7 after injury, staining was observed in stress fracture callus, especially in areas within newly formed bone near the crack.

4. Discussion

Our work describes and compares gene transcription in intramembranous and endochondral ossification using RNA-seq during stress fracture and full fracture repair, respectively. Several reports have examined gene expression of endochondral [12–16] or intramembranous repair [18]. However, our study is unique in making direct comparisons between the gene expression in these two different repair processes. Furthermore, we took a wider breadth than previous work by tracking gene expression over several time points for each model. Through analysis of top DEGs, and enriched GO terms and pathways for each fracture modality, we described how these expression patterns differed and progressed through time. We also employed callus cellular phenotyping techniques to estimate cell types within callus throughout repair. Finally, we used IHC to confirm the presence of some immune cell types in callus and surrounding tissues.

Although some DEGs were shared between stress fracture and full fracture repair, each of these models shows a high level of distinct

Table 1
Top ten up- and down-regulated genes and fold change at each time point in stress and full fracture.

	Stress fracture									
	Hour 4		Day 1		Day 3		Day 5		Day 7	
	Gene	FC	Gene	FC	Gene	FC	Gene	FC	Gene	FC
Up-regulated	Rrad	4.8	Timp1	6.7	C1qtnf3	24.8	Panx3	88.2	Panx3	24.2
	Ptgs2	4.7	Rrad	6.7	Panx3	20.7	C1qtnf3	75.0	C1qtnf3	20.9
	Socs3	4.7	Mmp3	5.2	Ptgs2	17.3	Col9a3	65.3	Car12	19.3
	Wnt1	4.2	Has2	5.1	Hapln4	13.3	Col9a2	62.8	Col10a1	14.0
	Ngf	4.1	Scn5a	4.9	Cthrc1	12.8	Col9a1	35.2	Col9a2	13.1
	Tnfrsf12a	3.6	Socs3	4.5	Tubb3	11.9	Hapln1	35.0	Col2a1	9.5
	Adamts4	3.6	Pdpn	4.4	Timp1	11.5	Ptgs2	34.7	Cthrc1	9.5
	Gm42679	3.5	Card14	4.4	Car12	11.4	Col2a1	34.3	Col9a3	9.4
	Has1	3.4	Myog	4.3	Acan	9.7	Car12	27.3	Myh8	8.9
	Serpine1	3.1	Adamts4	4.1	Fkbp11	8.7	Acan	24.0	Bcan	8.5
Down-regulated	Gng8	−2.5	Nell2	−2.4	Redrum	−3.8	Cd8b1	−5.2	Ighv9–3	−3.6
	Krt75	−2.4	A930018M24Rik	−2.3	Hist3h2ba	−3.7	Phyhip	−3.6	Phyhip	−3.3
	Dkk1	−2.4	Prss55	−2.3	F930017D23Rik	−3.7	Acmsd	−3.4	Hbb-bs	−3.2
	Dlx6os1	−2.4	Klhl33	−2.3	Inmt	−3.6	Gm42870	−3.4	Ms4a1	−3.2
	A530020G20Rik	−2.3	Ces1d	−2.2	A730036I17Rik	−3.6	Terc	−3.4	Fcmr	−3.1
	Gprasp2	−2.3	Sost	−2.2	Rhag	−3.6	Odf3l2	−3.4	Hbb-bt	−3.1
	Hrk	−2.3	Mylk4	−2.2	Klhl14	−3.6	Redrum	−3.3	RP23-171B16.2	−3.0
	Megf6	−2.3	Klf15	−2.1	Sowaha	−3.6	Rhag	−3.3	Alas2	−3.0
	Wscd2	−2.2	Asb15	−2.0	Hbb-bs	−3.5	2810030D12Rik	−3.3	Iglc2	−3.0
	Kcnk3	−2.2	Abca6	−2.0	Hbq1b	−3.5	Hemgn	−3.3	Cacna1i	−3.0

	Full fracture									
	Hour 4		Day 1		Day 3		Day 7		Day 14	
	Gene	FC	Gene	FC	Gene	FC	Gene	FC	Gene	FC
Up-regulated	Cxcl2	328.2	Arg1	234.3	Gm7325	73.7	Col9a1	440.5	Col10a1	97.0
	Cxcl1	276.9	Il11	188.9	Arg1	59.0	Ucma	437.9	Clec3a	54.0
	Csf3	275.0	Cxcl3	172.2	Tmem8c	56.0	Matn3	434.3	Panx3	47.0
	Il6	183.8	Cxcl2	81.4	Chrng	47.6	Lect1	415.2	3110079O15Rik	43.1
	Cxcl3	167.8	Ccl7	63.1	Il11	47.3	Clec3a	392.6	R3hdml	39.8
	Fosb	77.5	Ptgs2	49.1	Steap1	43.3	Col9a3	375.2	Col9a1	32.4
	Krt81	68.7	Ccl2	46.9	Pkhd1	38.5	Col10a1	328.1	Matn1	27.3
	Irg1	57.4	Spint1	32.1	Has2	35.9	Mfi2	320.7	Col9a2	27.0
	Ptgs2	55.5	Cxcl1	29.9	Ptgs2	35.6	Matn1	316.3	Mfi2	25.7
	Ccl2	51.6	Cxcl5	24.1	R3hdml	29.9	Col9a2	279.9	Lect1	24.8
Down-regulated	9430073C21Rik	−13.3	Cyp2e1	−30.0	Myl3	−44.0	Gp6	−43.1	Cyp2e1	−24.9
	Pck1	−10.4	Lrrc52	−19.3	Myl2	−40.8	Gm43291	−42.3	Ly6g6f	−23.9
	Gm28653	−9.9	Timp4	−13.5	Myh7	−31.8	Ly6g6f	−39.6	Gp6	−21.5
	Adrb3	−9.6	Aqp4	−13.3	Gm37527	−28.4	Ppbp	−37.6	G6b	−20.8
	Sln	−9.2	Col6a6	−12.5	Rp1	−25.4	Slamf1	−36.9	Mpl	−20.2
	Zic3	−8.1	Mylk4	−12.3	BC048679	−24.4	G6b	−36.8	Serpina3b	−19.5
	Dlx6os1	−8.1	A530016L24Rik	−12.2	Lrrc52	−24.2	Treml1	−35.1	Gm34302	−18.9
	Gm10629	−7.9	Lgi1	−11.9	Sowaha	−23.6	Tubb1	−33.0	Gp9	−18.8
	A930016O22Rik	−7.7	Pck1	−11.1	Perm1	−22.7	Gm42870	−33.0	Ppbp	−17.7
	A530016L24Rik	−7.7	Ces1d	−11.1	F930017D23Rik	−22.3	Gp9	−32.5	Treml1	−17.0

DEGs. This suggests that some fundamental processes are necessary for bone repair regardless of injury type – but that endochondral and intramembranous bone formation also have many distinct processes not shared between these models. We observed gradual gene expression changes following stress fracture, with few DEGs at early time points (Fig. 4A). However, by day 3 a robust number of DEGs were present at levels that persisted through our final time point (day 7). Contrastingly, we observed immediate and drastic changes in gene expression following full fracture, with thousands of DEGs at early time points, which was sustained at high levels throughout observed time points (Fig. 4B). This higher differential expression following full fracture is likely due to the more extensive injury of full fracture, as well as the greater variety of cells involved in endochondral ossification as compared to intramembranous ossification.

A key difference in gene expression between stress and full fracture arises from the larger inflammatory reaction in full fracture injury. This is highlighted by GO terms and pathways uniquely enriched during full fracture repair such as "*inflammatory response*", "*immune response*", "*cellular response to interleukin-1*", "*NFκB signaling*" and "*Toll-like receptor signaling*". These results are indicative of a highly inflamed bone microenvironment following fracture, matching literature reports of the components and importance of the inflammatory phase of fracture repair [10,58]. Specifically, IL-1 [59,60] and NFκB [58] have already been studied in endochondral fracture repair and thus validate our highly enriched pathway analysis for these terms. However, our pathway analysis showed enriched genes associated with toll-like receptors, which haven't previously been studied during endochondral fracture. These receptors, based on other reports, could be involved in monocyte recruitment, osteoblast differentiation, and tissue repair – however, the specific role they play in fracture repair needs to be further explored [61,62].

Stress fracture repair also features inflammation, with GO terms and pathways such as "*response to cytokine*", "*TNF signaling pathway*", and "*Cytokine-cytokine receptor interaction*" shared between both injuries.

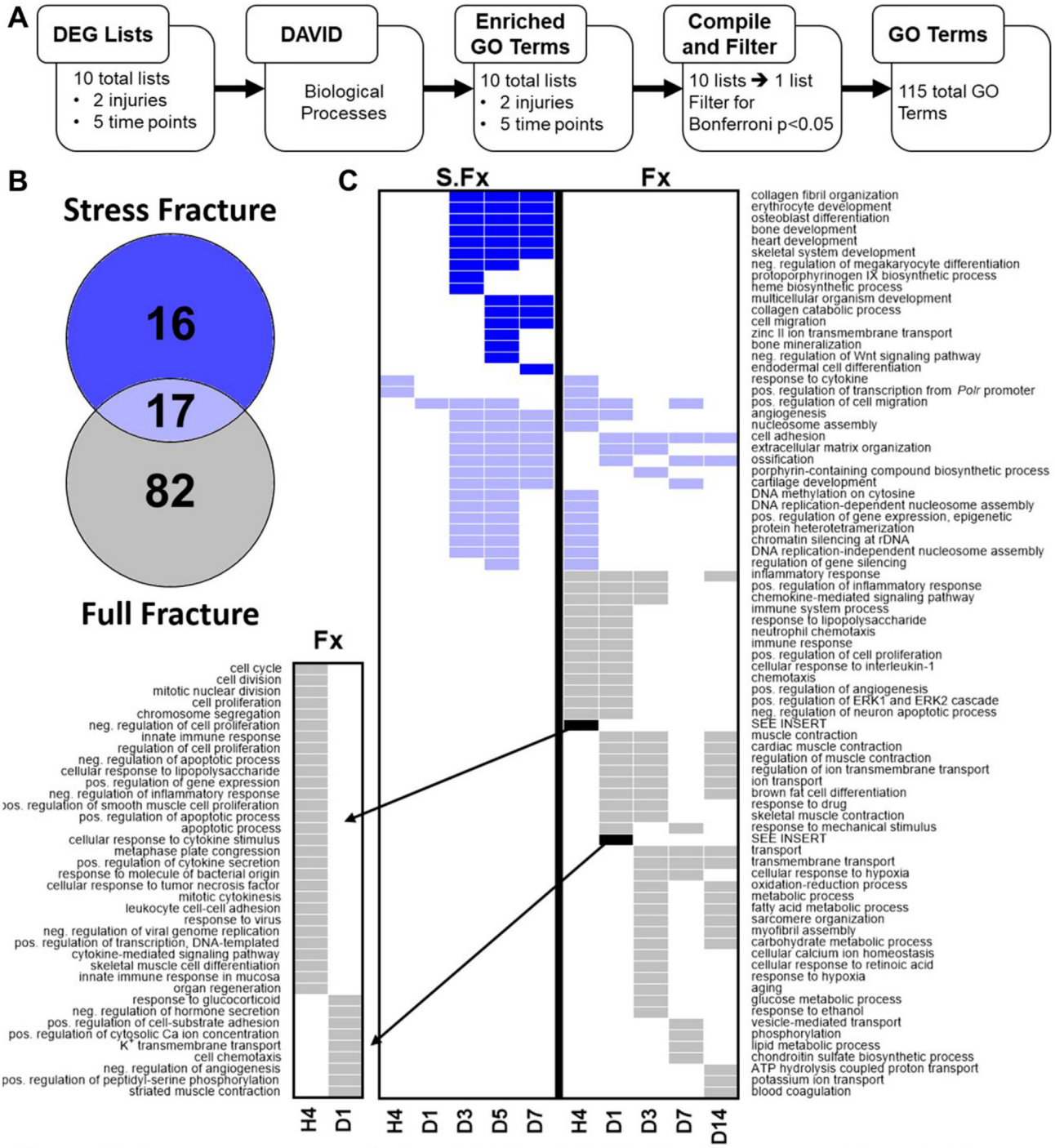

Fig. 5. Gene ontology analysis of DEGs. (A) Pipeline for gene ontology (GO) term analysis. (B) Comparison of the 115 GO terms uniquely enriched in stress fracture (dark blue), enriched in both injuries (light blue), or uniquely enriched in full fracture repair (grey). (C) Graphical list of all 115 enriched GO terms across all injuries and time points. Colors on chart match location of term from panel B. Go terms uniquely enriched in early full fracture time points were broken out into the smaller sub-panel for figure compactness (Black arrows). Blank spaces indicate GO term was not statistically enriched at time point or injury. H4 – 4 h, D1 – day 1, D3 – day 3, D5 – day 5, D7 – day 7, D14 – day 14. S.Fx - stress fracture, Fx - full fracture. (For interpretation of the references to color in this figure legend, the reader is referred to the web version of this article.)

This pattern of inflammation differs from that in microarray results of rat stress fracture reported by McKenzie et al., wherein IL-1, toll-like receptors, and NFκB were more prominently featured among DEGs [18]. Ptgs2 (aka Cox-2), a critical mediator of inflammation, was one of the most upregulated genes at several time points following stress fracture and full fracture (Table 1), and is a known contributor to successful healing [63,64]. Although it is certainly involved in stress fracture repair, the inflammatory reaction appears to be less extensive than after full fracture, both in terms of the numbers of relevant DEGS and their fold change.

The higher inflammation seen in the GO term and pathway analysis is also observed in callus cellular phenotyping and IHC analysis of fracture callus. Full fracture has a larger upregulation of immune-cell related genes as well as greater staining for Gr-1, F4/80, and CD45 than stress fracture (Figs. 7, 8). Recruitment of neutrophils, macrophages, and leukocytes to the site of injury at early time points is robust in our

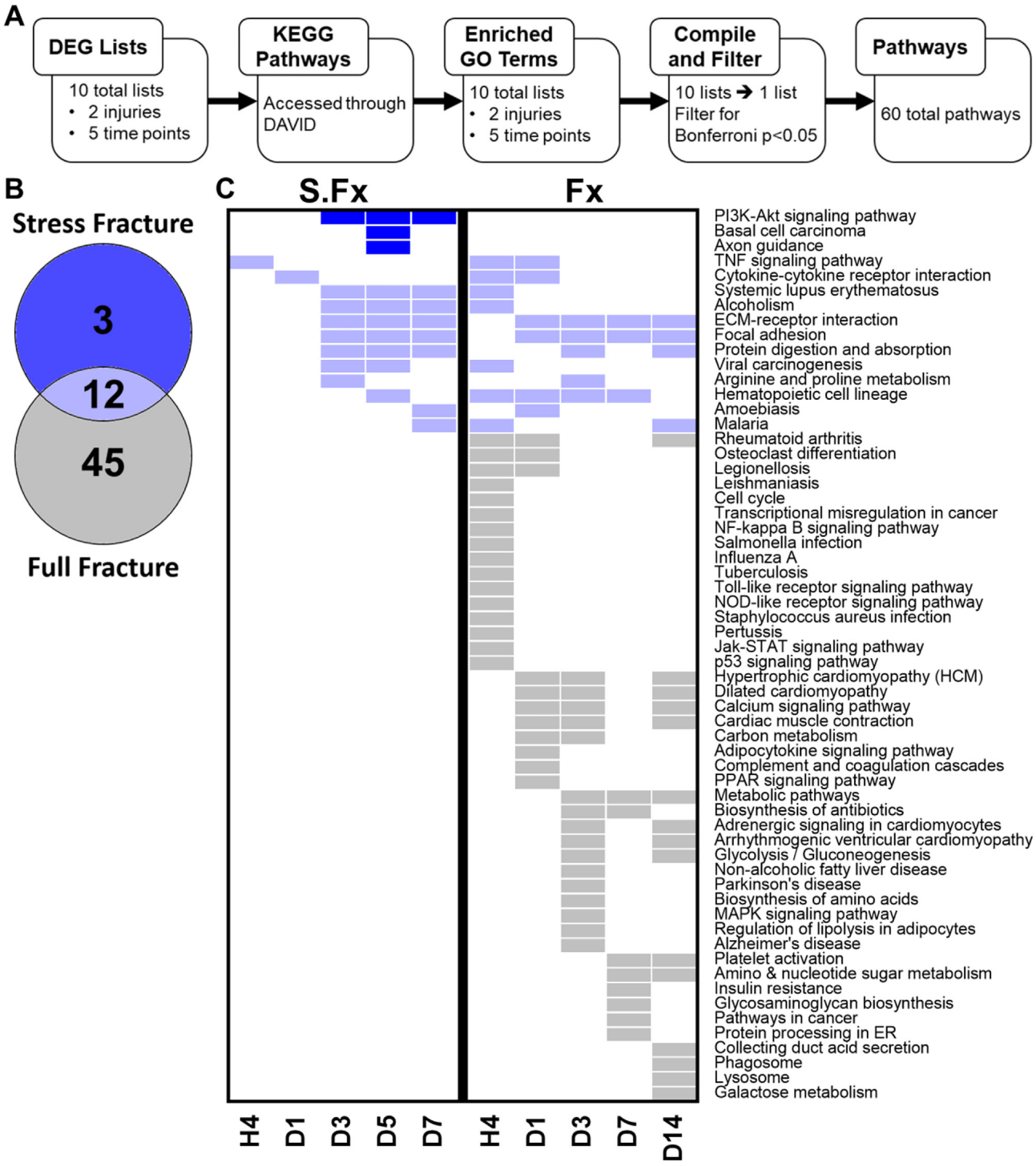

Fig. 6. Pathway analysis of DEGs. (A) Pipeline for pathway analysis. (B) Comparison of pathways enriched in stress and full fracture repair. (C) Graphical list of all 60 enriched pathways across injuries and time points. Colors on chart match location of pathway on panel B. Blank spaces indicate no significance of pathway at that time point/fracture condition. H4 – 4 h, D1 – day 1, D3 – day 3, D5 – day 5, D7 – day 7, D14 – day 14. S.Fx - stress fracture, Fx - full fracture. (For interpretation of the references to color in this figure legend, the reader is referred to the web version of this article.)

dataset. This is indicative of a healthy repair process, as these cells are important components of fracture repair [65–67]. Furthermore, IHC evidence of immune cell recruitment corroborates that the inflammatory signal in the RNA-seq data is functionally present in fracture repair at the cellular level. In addition, the callus phenotyping data showed an upregulation of T cell markers at early time points (hour 4 and day 1) following full fracture and to a lesser extent stress fracture. This is consistent with a report of T cell infiltration at early time points after full fracture [68]. But, how T cells impact fracture repair remains poorly understood. Reports show that elimination of the adaptive immune system benefits healing, but other reports show that elimination of certain subsets of T cells are detrimental to repair [69,70].

Our results indicate that stress fracture repair is a more direct model of post-injury osteogenesis. GO terms such as "*osteoblast development*", "*bone development*", "*skeletal system development*", and "*bone mineralization*" are uniquely enriched following stress fracture (Figs. 5 & 6).

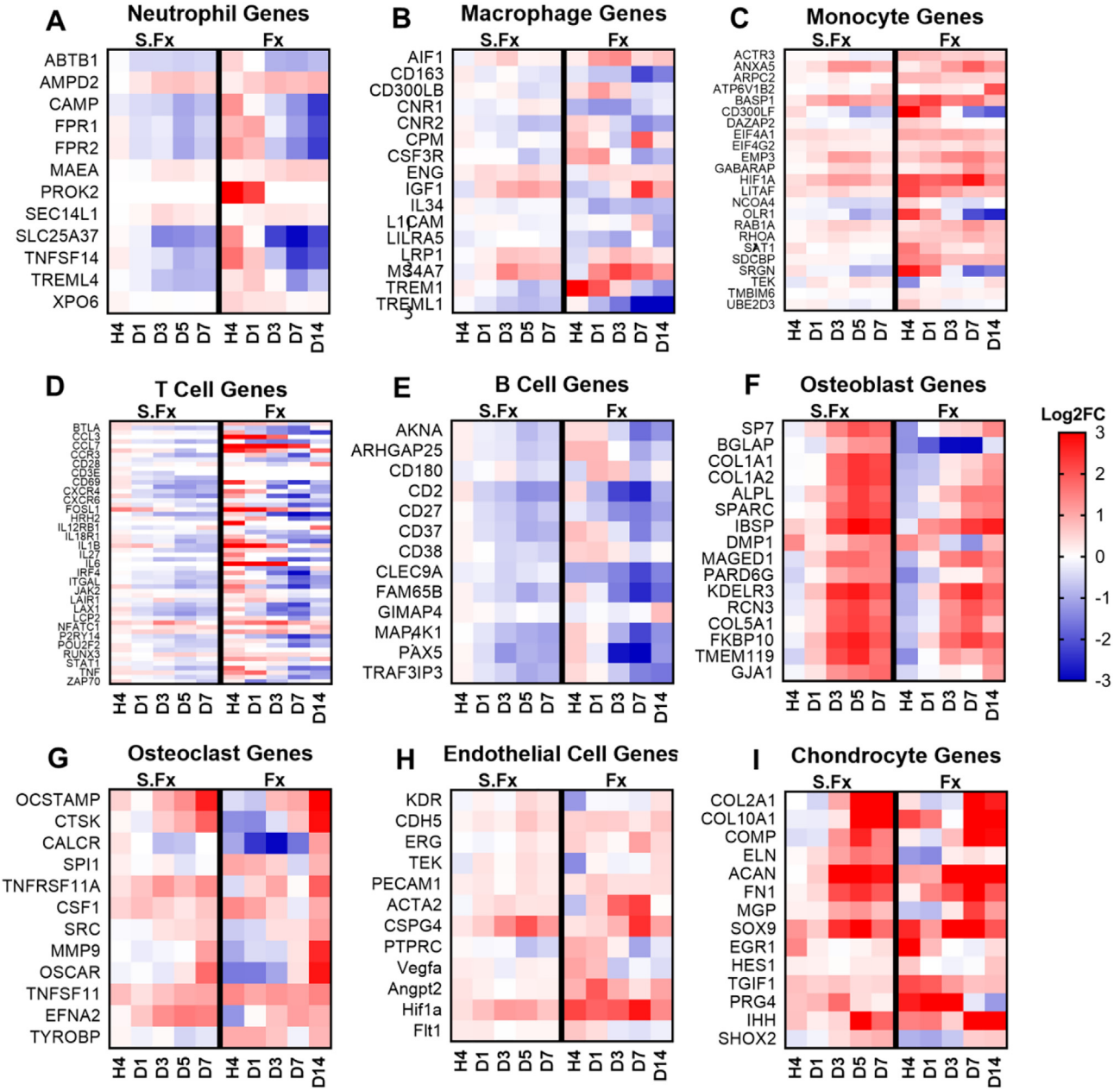

Fig. 7. Callus component phenotyping heat maps. Heat maps (log2 fold change) were generated for each time point and injury of curated genes lists associated with (A) Neutrophils, (B) Macrophages, (C) Monocytes, (D) T Cells, (E) B Cells, (F) Osteoblasts, (G) Osteoclasts, (H) Endothelial Cells, and (I) Chondrocytes. Gene lists were generated using literature sources in Supplementary Table 2.

Furthermore, in callus phenotyping, osteoblast associated genes are the strongest signal for any cell type following stress fracture (Fig. 7F). While full fracture is a mix of several important processes (i.e. osteogenesis, chondrogenesis, and inflammation), these additional processes can complicate interpretation of experiments designed to test defects in ossification. On the other hand, stress fracture repair involves fewer processes and cell types and therefor elicits strong enrichment of bone cell and osteogenic signals.

While stress fracture is a simplified model of post-injury osteogenesis, it elicits a distinctive and more complex transcriptional process than non-injurious anabolic bone formation. Kelly et al. used RNA-seq to determine expression changes in cortical bone following anabolic loading stimulation [71]. Few of the DEGs in their analysis were DEGs at similar time points following stress fracture (Supplementary Fig. 4). This agrees with previous reports showing stress fracture-induced intramembranous bone formation is transcriptionally distinct from loading-induced lamellar bone formation [18].

The PI3K-Akt signaling pathway is the only pathway uniquely enriched at multiple time points in stress fracture repair (Fig. 6). We also observed activation of this pathway in stress fracture callus using IHC (Supplementary Fig. 3). Interestingly, this pathway is important for osteoblast differentiation and function [72,73]. A few studies have examined this pathway in fracture repair. Qu et al. noted that inhibition of Akt signaling reduces MSC engraftment into fracture callus in a rescue model for rat non-union [74]. They further postulate that Akt signaling modulates post-injury osteogenesis via production of osteoprotegrin and bone gla protein. Furthermore, Scanlon et al. reported that PI3K can regulate thickening of the periosteum during the early stages of fracture repair [75]. These papers, along with our data, suggest PI3K-Akt signaling is an important and understudied component of bone regeneration.

Another difference between stress and full fracture repair is the host

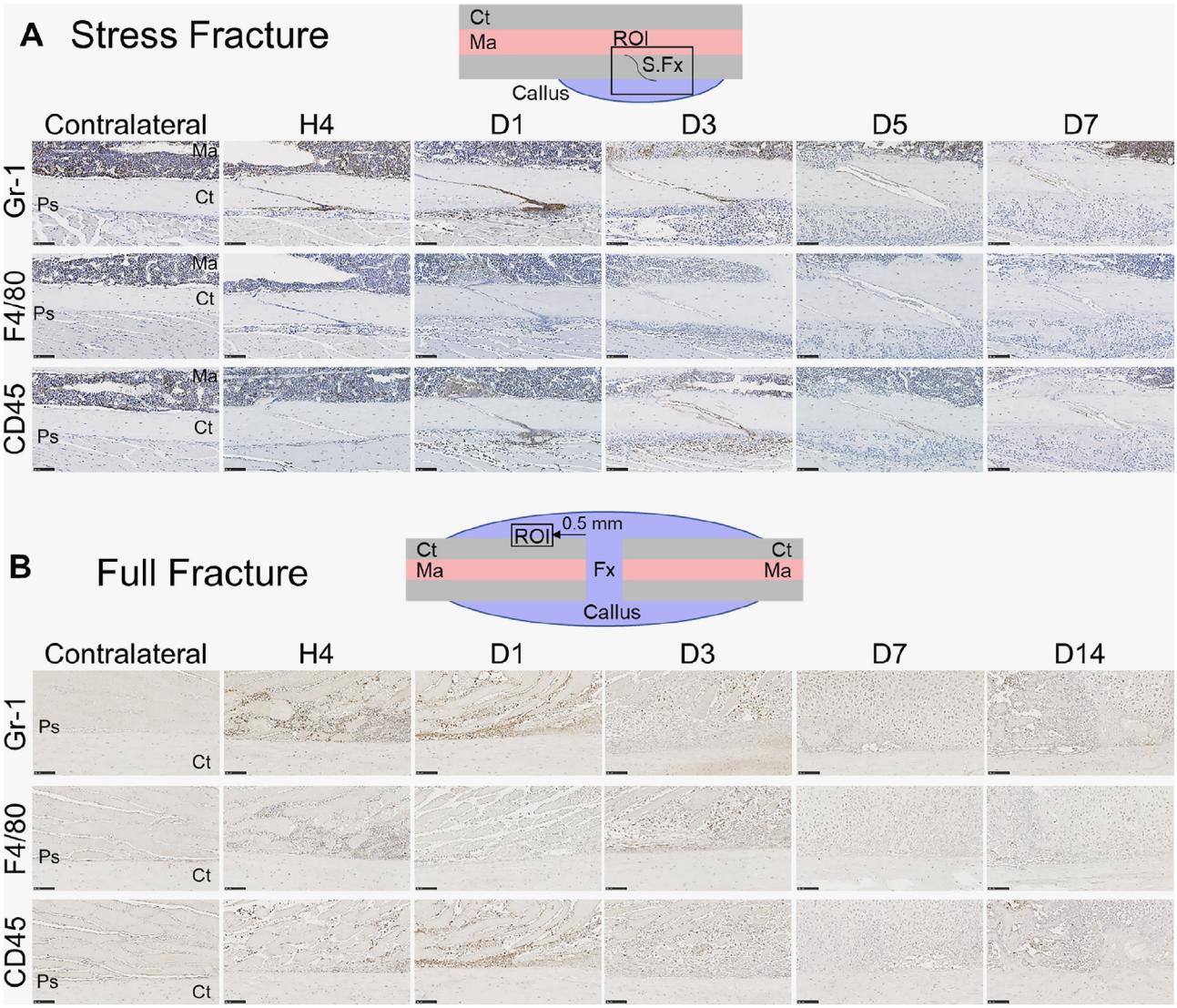

Fig. 8. Immune cell infiltration in fracture callus. Immunohistochemistry with antibodies for Gr-1, F4/80, and CD45 was used to stain for neutrophils, macrophages, and leukocytes, respectively. Cartoon depictions of the fracture callus show Region of interest (ROI) (Black box) in reference to (A) stress fracture (S.Fx) or (B) full fracture (Fx) location. All images are 20× magnifications and black scale bars are 100 μm. Ct = Cortical Bone, Ma = Marrow, Ps = Periosteum.

of ion transport-related GO terms ("*ion transport*", "*cellular calcium homeostasis*", "*potassium ion transmembrane transport*") and pathways ("*calcium signaling pathway*", "*cardiac muscle contraction*") which are uniquely enriched following full fracture. These terms were triggered by downregulation of calcium, potassium, and sodium voltage-gated channels (Fig. 9). One possibility for this downregulation includes ion channels directly influencing bone regeneration. Studies show ion channels involved in development and regeneration through endogenous bioelectrical patterning [76]. In fact, interfering with ion channels causes defective tail regeneration in amphibians [77]. Ion channels also have roles in bone cells, as potassium voltage gated channels regulate inflammation-induced bone resorption [78] and sodium voltage gated channels impact osteoblast function [79]. Reports of ion channels in bone repair have contradictory results [80,81] and would benefit from future exploration. The downregulation of ion channels could also involve pain sensation. Sodium, potassium, and calcium channels are components of pain sensation, and dysregulation of these channels result in painful neuropathies and hypersensitivities [82–84]. Furthermore, ion channels are downregulated in response to injury, contributing to post-injury mechanical hypersensitivity [85,86]. Whether ion channels impact fracture repair through either of these possible mechanisms or through a yet undiscussed mechanism, their downregulation is robust in full fracture repair and an appealing target for future study.

By using a contralateral control of intact bone, which is inherently enriched for bone cells, callus composed of a variety of cell types will have "differential expression" which is the result of different cellular composition in addition to true changes in gene expression of native cells. This should be kept in mind when considering the DEGs represented in this work as this likely limits our ability to capture expression changes of native bone cells. However, utilizing this as a feature of our whole callus sequencing allowed us to use callus cellular phenotyping to infer cell types present throughout fracture repair. Furthermore, it is possible that the surgery performed while initiating the full fracture could itself influence gene expression when comparing to a no surgery contralateral control. Despite this possibility, we believe that fracture is the primary driver of gene expression and is responsible for the large differential expression reported herein.

5. Conclusions

In this report the gene expression of bone repair is examined using

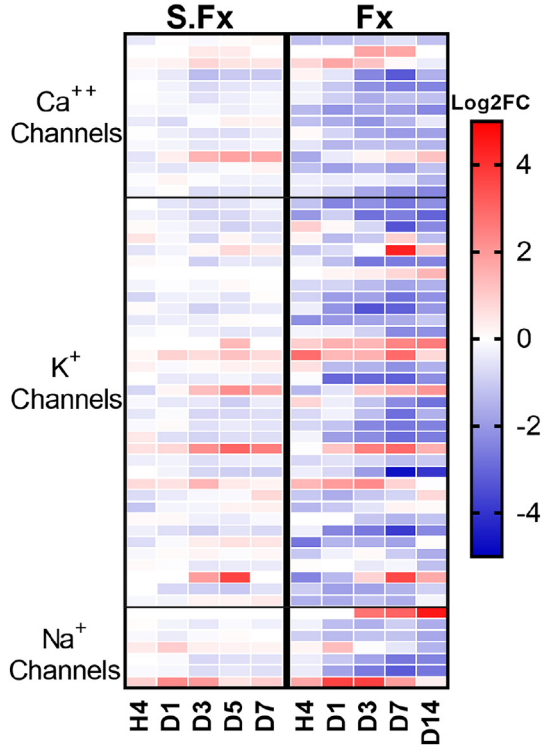

Fig. 9. Ion channels are downregulated following full fracture. The Log2 FC of Calcium, Potassium, and Sodium Voltage Gated Channels which were DEGs are displayed across all time points for stress fracture (S.FX) and full fracture (FX). These channels were disproportionally down-regulated throughout full fracture repair. Due to these down-regulated DEGs, Go terms and pathways such as "*ion transport*", "*cellular calcium homeostasis*", "*potassium ion transmembrane transport*", "*calcium signaling pathway*", and "*cardiac muscle contraction*" were enriched during full fracture repair. A full list of these genes is provided in Supplementary Table 4.

two models of murine fracture repair. Intramembranous repair, as modeled by ulnar stress fracture, and endochondral repair, as modeled by femur full fracture, exhibit vastly different transcriptional profiles throughout repair. Full fracture repair includes a much stronger inflammatory response and a down regulation in ion transporter genes not experienced in stress fracture repair. Within stress fracture repair is a strong signal of osteoblasts and osteogenesis which reflects a simpler repair process. These data offer a detailed description of gene transcription in bone fracture repair, and highlight several pathways and processes as potential new avenues of research that may lead to innovative solutions to clinical complications in fracture repair.

Acknowledgements

This work was supported by funding from NIAMS (R01 AR050211, P30 AR057235, and P30 AR074992) and NIBIB (T32 EB018266). The authors would like to thank the cores and staff of the Washington University Musculoskeletal Research Center for their assistance. Specifically, thanks to Crystal Idleburg and Samantha Coleman for histological processing and sectioning and Dan Leib for assistance in radiograph image acquisition. Histology slides were imaged with the Nanozoomer at Alafi Neuroimaging Core (S10 RR027552). RNA sequencing was performed by the Genome Technology Access Center in the Department of Genetics at Washington University School of Medicine which is partially supported by NCI (P30 CA91842) and NCRR (UL1 TR000448).

Author roles

Brandon Coates: Conceptualization, Formal Analysis, Investigation, Data Curation, Writing –Original Draft, Writing – Review & Editing, Visualization. **Jennifer McKenzie**: Conceptualization, Investigation, Writing –Original Draft, Writing – Review & Editing. **Evan Buettmann**: Investigation, Writing – Review & Editing. **Xiaochen Liu**: Investigation, Writing – Review & Editing. **Paul Gontarz**: Software, Formal Analysis, Data Curation. **Bo Zhang**: Software, Formal Analysis, Data Curation, Writing – Review & Editing. **Matthew Silva**: Conceptualization, Resources, Writing –Original Draft, Writing – Review & Editing, Supervision, Funding Acquisition.

Declaration of competing interest

The authors would like to disclose that Matthew Silva has past research grant support from Merck Co. (2014–2017) and occasional royalty income from Springer.

All other authors have no financial conflicts of interest with the submission of this manuscript.

Appendix A. Supplementary data

Supplementary data to this article can be found online at https://doi.org/10.1016/j.bone.2019.07.022.

References

[1] W.-C. Pollak, Andrew N. Sylvia I., Fracture trends, in: United States Bone and Joint Initiative: The Burden of Musculoskeletal Diseases in the United States (BMUS), Third edition, 2014, Rosemont, IL, n.d. http://www.boneandjointburden.org/ (accessed November 13, 2018).

[2] R. Zura, Z. Xiong, T. Einhorn, J.T. Watson, R.F. Ostrum, M.J. Prayson, G.J. Della Rocca, S. Mehta, T. McKinley, Z. Wang, R.G. Steen, Epidemiology of fracture nonunion in 18 human bones, JAMA Surg. 151 (2016) e162775, , https://doi.org/10.1001/jamasurg.2016.2775.

[3] M.S. Gaston, A.H.R.W. Simpson, Inhibition of fracture healing, J. Bone Joint Surg.. British Volume. 89-B (2007) 1553–1560. doi:https://doi.org/10.1302/0301-620X.89B12.19671.

[4] M. Pepper, V. Akuthota, E.C. McCarty, The pathophysiology of stress fractures, Clin. Sports Med. 25 (2006) 1–16, https://doi.org/10.1016/j.csm.2005.08.010.

[5] S.J. Warden, D.B. Burr, P.D. Brukner, Stress Fractures: Pathophysiology, Epidemiology, and Risk Factors, (n.d.) 7.

[6] M. Schaffler, Bone fatigue and remodeling in the devlopment of stress fractures, in: D. Burr, C. Milgrom (Eds.), Musculoskeletal Fatigue and Stress Fractures, CRC Press, Boca Raton, 2000, pp. 161–182.

[7] K.L. Bennell, P.D. Brukner, Epidemiology and site specificity of stress fractures, Clin. Sports Med. 16 (1997) 179–196, https://doi.org/10.1016/S0278-5919(05)70016-8.

[8] F. Bonnarens, T.A. Einhorn, Production of a standard closed fracture in laboratory animal bone, J. Orthop. Res. 2 (1984) 97–101, https://doi.org/10.1002/jor.1100020115.

[9] Z. Thompson, T. Miclau, D. Hu, J.A. Helms, A model for intramembranous ossification during fracture healing, J. Orthop. Res. 20 (2002) 1091–1098, https://doi.org/10.1016/S0736-0266(02)00017-7.

[10] L.C. Gerstenfeld, D.M. Cullinane, G.L. Barnes, D.T. Graves, T.A. Einhorn, Fracture healing as a post-natal developmental process: molecular, spatial, and temporal aspects of its regulation, J. Cell. Biochem. 88 (2003) 873–884, https://doi.org/10.1002/jcb.10435.

[11] R. Marsell, T.A. Einhorn, The biology of fracture healing, Injury 42 (2011) 551–555, https://doi.org/10.1016/j.injury.2011.03.031.

[12] J.H. Hebb, J.W. Ashley, L. McDaniel, L.A. Lopas, J. Tobias, K.D. Hankenson, J. Ahn, Bone healing in an aged murine fracture model is characterized by sustained callus inflammation and decreased cell proliferation: fracture healing in aged mice, J. Orthop. Res. (2017), https://doi.org/10.1002/jor.23652.

[13] C. Yuan, J. Cai, Time-series expression profile analysis of fracture healing in young and old mice, Mol. Med. Rep. 16 (2017) 4529–4536, https://doi.org/10.3892/mmr.2017.7198.

[14] R. Grimes, K.J. Jepsen, J.L. Fitch, T.A. Einhorn, L.C. Gerstenfeld, The transcriptome of fracture healing defines mechanisms of coordination of skeletal and vascular development during endochondral bone formation, J. Bone Miner. Res. 26 (2011) 2597–2609, https://doi.org/10.1002/jbmr.486.

[15] C.H. Rundle, H. Wang, H. Yu, R.B. Chadwick, E.I. Davis, J.E. Wergedal, K.-H.W. Lau, S. Mohan, J.T. Ryaby, D.J. Baylink, Microarray analysis of gene expression during the inflammation and endochondral bone formation stages of rat femur fracture repair, Bone 38 (2006) 521–529, https://doi.org/10.1016/j.bone.2005.09.015.

[16] G. Zimmermann, K.H.K. Schmeckenbecher, S. Boeuf, S. Weiss, R. Bock, A. Moghaddam, W. Richter, Differential gene expression analysis in fracture callus of patients with regular and failed bone healing, Injury 43 (2012) 347–356, https://doi.org/10.1016/j.injury.2011.10.031.

[17] M. Hauser, M. Siegrist, I. Keller, W. Hofstetter, Healing of fractures in osteoporotic bones in mice treated with bisphosphonates - a transcriptome analysis, Bone 112 (2018) 107–119, https://doi.org/10.1016/j.bone.2018.04.017.

[18] J.A. McKenzie, E.C. Bixby, M.J. Silva, Differential gene expression from microarray analysis distinguishes woven and lamellar bone formation in the rat ulna following mechanical loading, PLoS One 6 (2011) e29328, , https://doi.org/10.1371/journal.pone.0029328.

[19] K.M. Sanders, E. Seeman, A.M. Ugoni, J.A. Pasco, T.J. Martin, B. Skoric, G.C. Nicholson, M.A. Kotowicz, Age- and gender-specific rate of fractures in Australia: a population-based study, Osteoporos. Int. 10 (1999) 240–247, https://doi.org/10.1007/s001980050222.

[20] S.R. Cummings, L.J. Melton, Epidemiology and outcomes of osteoporotic fractures, Lancet 359 (2002) 1761–1767, https://doi.org/10.1016/S0140-6736(02)08657-9.

[21] S.H. McBride-Gagyi, J.A. McKenzie, E.G. Buettmann, M.J. Gardner, M.J. Silva, Bmp2 conditional knockout in osteoblasts and endothelial cells does not impair bone formation after injury or mechanical loading in adult mice, Bone 81 (2015) 533–543, https://doi.org/10.1016/j.bone.2015.09.003.

[22] M.D. Martinez, G.J. Schmid, J.A. McKenzie, D.M. Ornitz, M.J. Silva, Healing of non-displaced fractures produced by fatigue loading of the mouse ulna, Bone 46 (2010) 1604–1612, https://doi.org/10.1016/j.bone.2010.02.030.

[23] X. Liu, J.A. McKenzie, C.W. Maschhoff, M.J. Gardner, M.J. Silva, Exogenous hedgehog antagonist delays but does not prevent fracture healing in young mice, Bone 103 (2017) 241–251, https://doi.org/10.1016/j.bone.2017.07.017.

[24] D.W. Huang, B.T. Sherman, R.A. Lempicki, Systematic and integrative analysis of large gene lists using DAVID bioinformatics resources, Nat. Protoc. 4 (2009) 44–57, https://doi.org/10.1038/nprot.2008.211.

[25] D.W. Huang, B.T. Sherman, R.A. Lempicki, Bioinformatics enrichment tools: paths toward the comprehensive functional analysis of large gene lists, Nucleic Acids Res. 37 (2009) 1–13, https://doi.org/10.1093/nar/gkn923.

[26] M. Angelova, P. Charoentong, H. Hackl, M.L. Fischer, R. Snajder, A.M. Krogsdam, M.J. Waldner, G. Bindea, B. Mlecnik, J. Galon, Z. Trajanoski, Characterization of the immunophenotypes and antigenomes of colorectal cancers reveals distinct tumor escape mechanisms and novel targets for immunotherapy, Genome Biol. 16 (2015), https://doi.org/10.1186/s13059-015-0620-6.

[27] G. Calabrese, B.J. Bennett, L. Orozco, H.M. Kang, E. Eskin, C. Dombret, O. De Backer, A.J. Lusis, C.R. Farber, Systems genetic analysis of osteoblast-lineage cells, PLoS Genet. 8 (2012) e1003150, , https://doi.org/10.1371/journal.pgen.1003150.

[28] G.A. Rodan, M. Noda, Gene expression in osteoblastic cells, Crit. Rev. Eukaryot. Gene Expr. 1 (1991) 85–98.

[29] A.D. Barrow, N. Raynal, T.L. Andersen, D.A. Slatter, D. Bihan, N. Pugh, M. Cella, T. Kim, J. Rho, T. Negishi-Koga, J.-M. Delaisse, H. Takayanagi, J. Lorenzo, M. Colonna, R.W. Farndale, Y. Choi, J. Trowsdale, OSCAR is a collagen receptor that costimulates osteoclastogenesis in DAP12-deficient humans and mice, J. Clin. Invest. 121 (2011) 3505–3516, https://doi.org/10.1172/JCI45913.

[30] N. Irie, Y. Takada, Y. Watanabe, Y. Matsuzaki, C. Naruse, M. Asano, Y. Iwakura, T. Suda, K. Matsuo, Bidirectional signaling through ephrinA2-EphA2 enhances osteoclastogenesis and suppresses osteoblastogenesis, J. Biol. Chem. 284 (2009) 14637–14644, https://doi.org/10.1074/jbc.M807598200.

[31] J. Jiang, H. Li, F.S. Fahid, E. Filbert, K.E. Safavi, L.S. Spangberg, Q. Zhu, Quantitative analysis of osteoclast-specific gene markers stimulated by lipopolysaccharide, J. Endod. 32 (2006) 742–746, https://doi.org/10.1016/j.joen.2006.02.003.

[32] M. Yang, M.J. Birnbaum, C.A. MacKay, A. Mason-Savas, B. Thompson, P.R. Odgren, Osteoclast stimulatory transmembrane protein (OC-STAMP), a novel protein induced by RANKL that promotes osteoclast differentiation, J. Cell. Physiol. 215 (2008) 497–505, https://doi.org/10.1002/jcp.21331.

[33] M. Zaidi, H.C. Blair, B.S. Moonga, E. Abe, C.L.-H. Huang, Osteoclastogenesis, bone resorption, and osteoclast-based therapeutics, J. Bone Miner. Res. 18 (2003) 599–609, https://doi.org/10.1359/jbmr.2003.18.4.599.

[34] C.G. Rivera, S. Mellberg, L. Claesson-Welsh, J.S. Bader, A.S. Popel, Analysis of VEGF-a regulated gene expression in endothelial cells to identify genes linked to angiogenesis, PLoS One 6 (2011) e24887, , https://doi.org/10.1371/journal.pone.0024887.

[35] M.F. Sabbagh, J.S. Heng, C. Luo, R.G. Castanon, J.R. Nery, A. Rattner, L.A. Goff, J.R. Ecker, J. Nathans, Transcriptional and epigenomic landscapes of CNS and non-CNS vascular endothelial cells, Elife 7 (2018), https://doi.org/10.7554/eLife.36187.

[36] T. Dehne, R. Schenk, C. Perka, L. Morawietz, A. Pruss, M. Sittinger, C. Kaps, J. Ringe, Gene expression profiling of primary human articular chondrocytes in high-density micromasses reveals patterns of recovery, maintenance, re- and dedifferentiation, Gene 462 (2010) 8–17, https://doi.org/10.1016/j.gene.2010.04.006.

[37] F.-T. Xu, H.-M. Li, C.-Y. Zhao, Z.-J. Liang, M.-H. Huang, Q. Li, Y.-C. Chen, G.-Y. Chi, Characterization of chondrogenic gene expression and cartilage phenotype differentiation in human breast adipose-derived stem cells promoted by ginsenoside Rg1 in vitro, Cell. Physiol. Biochem. 37 (2015) 1890–1902, https://doi.org/10.1159/000438550.

[38] L. Yu, H. Liu, M. Yan, J. Yang, F. Long, K. Muneoka, Y. Chen, Shox2 is required for chondrocyte proliferation and maturation in proximal limb skeleton, Dev. Biol. 306 (2007) 549–559, https://doi.org/10.1016/j.ydbio.2007.03.518.

[39] Y.-C. Lin, S.R. Roffler, Y.-T. Yan, R.-B. Yang, Disruption of Scube2 impairs endochondral bone formation, J. Bone Miner. Res. 30 (2015) 1255–1267, https://doi.org/10.1002/jbmr.2451.

[40] C.N. Withers, D.M. Brown, I. Byiringiro, M.R. Allen, K.W. Condon, J. Satin, D.A. Andres, Rad GTPase is essential for the regulation of bone density and bone marrow adipose tissue in mice, Bone 103 (2017) 270–280, https://doi.org/10.1016/j.bone.2017.07.018.

[41] F. Paic, J.C. Igwe, R. Nori, M.S. Kronenberg, T. Franceschetti, P. Harrington, L. Kuo, D.-G. Shin, D.W. Rowe, S.E. Harris, I. Kalajzic, Identification of differentially expressed genes between osteoblasts and osteocytes, Bone 45 (2009) 682–692, https://doi.org/10.1016/j.bone.2009.06.010.

[42] S.R. Bond, A. Lau, S. Penuela, A.V. Sampaio, T.M. Underhill, D.W. Laird, C.C. Naus, Pannexin 3 is a novel target for Runx2, expressed by osteoblasts and mature growth plate chondrocytes, J. Bone Miner. Res. 26 (2011) 2911–2922, https://doi.org/10.1002/jbmr.509.

[43] M. Ishikawa, Y. Yamada, The role of Pannexin 3 in bone biology, J. Dent. Res. 96 (2017) 372–379, https://doi.org/10.1177/0022034516678203.

[44] Y. Zhou, J.-Y. Wang, H. Feng, C. Wang, L. Li, D. Wu, H. Lei, H. Li, L.-L. Wu, Overexpression of C1q/Tumor Necrosis Factor–related Protein-3 Promotes Phosphate-induced Vascular Smooth Muscle Cell Calcification Both In Vivo and In Vitro, Arteriosclerosis, Thrombosis, and Vascular Biology, 34 (2014), pp. 1002–1010, https://doi.org/10.1161/ATVBAHA.114.303301.

[45] A.K. Coussens, C.R. Wilkinson, I.P. Hughes, C.P. Morris, A. van Daal, P.J. Anderson, B.C. Powell, Unravelling the molecular control of calvarial suture fusion in children with craniosynostosis, BMC Genomics 8 (2007) 458, https://doi.org/10.1186/1471-2164-8-458.

[46] G.R. Wohl, D.A. Towler, M.J. Silva, Stress fracture healing: fatigue loading of the rat ulna induces upregulation in expression of osteogenic and angiogenic genes that mimic the intramembranous portion of fracture repair, Bone 44 (2009) 320–330, https://doi.org/10.1016/j.bone.2008.09.010.

[47] P. Fedi, A. Bafico, A.N. Soria, W.H. Burgess, T. Miki, D.P. Bottaro, M.H. Kraus, S.A. Aaronson, Isolation and biochemical characterization of the human Dkk-1 homologue, a novel inhibitor of mammalian Wnt signaling, J. Biol. Chem. 274 (1999) 19465–19472, https://doi.org/10.1074/jbc.274.27.19465.

[48] X. Li, Y. Zhang, H. Kang, W. Liu, P. Liu, J. Zhang, S.E. Harris, D. Wu, Sclerostin binds to LRP5/6 and antagonizes canonical Wnt signaling, J. Biol. Chem. 280 (2005) 19883–19887, https://doi.org/10.1074/jbc.M413274200.

[49] D.S. Bischoff, T. Sakamoto, K. Ishida, N.S. Makhijani, H.E. Gruber, D.T. Yamaguchi, CXC receptor knockout mice: characterization of skeletal features and membranous bone healing in the adult mouse, Bone 48 (2011) 267–274, https://doi.org/10.1016/j.bone.2010.09.026.

[50] K.J. Eash, A.M. Greenbaum, P.K. Gopalan, D.C. Link, CXCR2 and CXCR4 antagonistically regulate neutrophil trafficking from murine bone marrow, J. Clin. Investig. 120 (2010) 2423–2431, https://doi.org/10.1172/JCI41649.

[51] J.A. Belperio, M.P. Keane, D.A. Arenberg, C.L. Addison, J.E. Ehlert, M.D. Burdick, R.M. Strieter, CXC chemokines in angiogenesis, J. Leukoc. Biol. 68 (2000) 1–8, https://doi.org/10.1189/jlb.68.1.1.

[52] A. Wallace, T.E. Cooney, R. Englund, J.D. Lubahn, Effects of Interleukin-6 ablation on fracture healing in mice, J. Orthop. Res. 29 (2011) 1437–1442, https://doi.org/10.1002/jor.21367.

[53] X. Yang, B.F. Ricciardi, A. Hernandez-Soria, Y. Shi, N. Pleshko Camacho, M.P.G. Bostrom, Callus mineralization and maturation are delayed during fracture healing in interleukin-6 knockout mice, Bone 41 (2007) 928–936, https://doi.org/10.1016/j.bone.2007.07.022.

[54] A.M. Simon, M.B. Manigrasso, J.P. O'Connor, Cyclo-oxygenase 2 function is essential for bone fracture healing, J. Bone Miner. Res. 17 (2002) 963–976, https://doi.org/10.1359/jbmr.2002.17.6.963.

[55] L.C. Gerstenfeld, M. Thiede, K. Seibert, C. Mielke, D. Phippard, B. Svagr, D. Cullinane, T.A. Einhorn, Differential inhibition of fracture healing by non-selective and cyclooxygenase-2 selective non-steroidal anti-inflammatory drugs, J. Orthop. Res. 21 (2003) 670–675, https://doi.org/10.1016/S0736-0266(03)00003-2.

[56] Y. Takeuchi, S. Watanabe, G. Ishii, S. Takeda, K. Nakayama, S. Fukumoto, Y. Kaneta, D. Inoue, T. Matsumoto, K. Harigaya, T. Fujita, Interleukin-11 as a stimulatory factor for bone formation prevents bone loss with advancing age in mice, J. Biol. Chem. 277 (2002) 49011–49018, https://doi.org/10.1074/jbc.M207804200.

[57] L. Campbell, C.R. Saville, P.J. Murray, S.M. Cruickshank, M.J. Hardman, Local arginase 1 activity is required for cutaneous wound healing, J. Invest. Dermatol. 133 (2013) 2461–2470, https://doi.org/10.1038/jid.2013.164.

[58] T. Kon, T.-J. Cho, T. Aizawa, M. Yamazaki, N. Nooh, D. Graves, L.C. Gerstenfeld, T.A. Einhorn, Expression of osteoprotegerin, receptor activator of NF-κB ligand (osteoprotegerin ligand) and related proinflammatory cytokines during fracture healing, J. Bone Miner. Res. 16 (2001) 1004–1014, https://doi.org/10.1359/jbmr.2001.16.6.1004.

[59] D.N. Tatakis, Interleukin-1 and bone metabolism: a review, J. Periodontol. 64 (1993) 416–431.

[60] X. Wang, T.E. Friis, P.P. Masci, R.W. Crawford, W. Liao, Y. Xiao, Alteration of blood clot structures by interleukin-1 beta in association with bone defects healing, Sci. Rep. 6 (2016), https://doi.org/10.1038/srep35645.

[61] M. Li, D.F. Carpio, Y. Zheng, P. Bruzzo, V. Singh, F. Ouaaz, R.M. Medzhitov, A.A. Beg, An essential role of the NF-B/toll-like receptor pathway in induction of inflammatory and tissue-repair gene expression by necrotic cells, J. Immunol. 166 (2001) 7128–7135, https://doi.org/10.4049/jimmunol.166.12.7128.

[62] C. Shi, T. Jia, S. Mendez-Ferrer, T.M. Hohl, N.V. Serbina, L. Lipuma, I. Leiner, M.O. Li, P.S. Frenette, E.G. Pamer, Bone marrow mesenchymal stem and progenitor cells induce monocyte emigration in response to circulating toll-like receptor ligands, Immunity 34 (2011) 590–601, https://doi.org/10.1016/j.immuni.2011.02.016.

[63] L.J. Kidd, N.R. Cowling, A.C. Wu, W.L. Kelly, M.R. Forwood, Selective and non-selective cyclooxygenase inhibitors delay stress fracture healing in the rat ulna, J. Orthop. Res. 31 (2013) 235–242, https://doi.org/10.1002/jor.22203.
[64] X. Zhang, E.M. Schwarz, D.A. Young, J.E. Puzas, R.N. Rosier, R.J. O'Keefe, Cyclooxygenase-2 regulates mesenchymal cell differentiation into the osteoblast lineage and is critically involved in bone repair, J. Clin. Investig. 109 (2002) 1405–1415, https://doi.org/10.1172/JCI15681.
[65] A. Kovtun, S. Bergdolt, R. Wiegner, P. Radermacher, M. Huber-Lang, A. Ignatius, The crucial role of neutrophil granulocytes in bone fracture healing, Eur. Cell. Mater. 32 (2016) 152–162.
[66] C. Schlundt, T. El Khassawna, A. Serra, A. Dienelt, S. Wendler, H. Schell, N. van Rooijen, A. Radbruch, R. Lucius, S. Hartmann, G.N. Duda, K. Schmidt-Bleek, Macrophages in bone fracture healing: their essential role in endochondral ossification, Bone 106 (2018) 78–89, https://doi.org/10.1016/j.bone.2015.10.019.
[67] S. Levy, J.M. Feduska, A. Sawant, S.R. Gilbert, J.A. Hensel, S. Ponnazhagan, Immature myeloid cells are critical for enhancing bone fracture healing through angiogenic cascade, Bone 93 (2016) 113–124, https://doi.org/10.1016/j.bone.2016.09.018.
[68] P. Hoff, T. Gaber, C. Strehl, K. Schmidt-Bleek, A. Lang, D. Huscher, G.R. Burmester, G. Schmidmaier, C. Perka, G.N. Duda, F. Buttgereit, Immunological characterization of the early human fracture hematoma, Immunol. Res. 64 (2016) 1195–1206, https://doi.org/10.1007/s12026-016-8868-9.
[69] T. Ono, K. Okamoto, T. Nakashima, T. Nitta, S. Hori, Y. Iwakura, H. Takayanagi, IL-17-producing γδ T cells enhance bone regeneration, Nat. Commun. 7 (2016), https://doi.org/10.1038/ncomms10928.
[70] D. Toben, I. Schroeder, T. El Khassawna, M. Mehta, J.-E. Hoffmann, J.-T. Frisch, H. Schell, J. Lienau, A. Serra, A. Radbruch, G.N. Duda, Fracture healing is accelerated in the absence of the adaptive immune system, J. Bone Miner. Res. 26 (2011) 113–124, https://doi.org/10.1002/jbmr.185.
[71] N.H. Kelly, J.C. Schimenti, F.P. Ross, M.C.H. van der Meulen, Transcriptional profiling of cortical versus cancellous bone from mechanically-loaded murine tibiae reveals differential gene expression, Bone 86 (2016) 22–29, https://doi.org/10.1016/j.bone.2016.02.007.
[72] A. Yang, Y. Lu, J. Xing, Z. Li, X. Yin, C. Dou, S. Dong, F. Luo, Z. Xie, T. Hou, J. Xu, IL-8 enhances therapeutic effects of BMSCs on bone regeneration via CXCR2-mediated PI3k/Akt signaling pathway, Cell. Physiol. Biochem. 48 (2018) 361–370, https://doi.org/10.1159/000491742.
[73] I.M. McGonnell, A.E. Grigoriadis, E.W.-F. Lam, J.S. Price, A. Sunters, A specific role for phosphoinositide 3-kinase and AKT in osteoblasts? Front. Endocrinol. (Lausanne) 3 (2012) 88, , https://doi.org/10.3389/fendo.2012.00088.
[74] Z. Qu, S. Guo, G. Fang, Z. Cui, Y. Liu, AKT pathway affects bone regeneration in nonunion treated with umbilical cord-derived mesenchymal stem cells, Cell Biochem. Biophys. 71 (2015) 1543–1551, https://doi.org/10.1007/s12013-014-0378-6.
[75] V. Scanlon, B. Walia, J. Yu, M. Hansen, H. Drissi, P. Maye, A. Sanjay, Loss of Cbl-PI3K interaction modulates the periosteal response to fracture by enhancing osteogenic commitment and differentiation, Bone 95 (2017) 124–135, https://doi.org/10.1016/j.bone.2016.11.020.
[76] M. Levin, Endogenous bioelectrical networks store non-genetic patterning information during development and regeneration: bioelectric networks as epi-genetic controls of growth and form, J. Physiol. 592 (2014) 2295–2305, https://doi.org/10.1113/jphysiol.2014.271940.
[77] B.M. Franklin, S.R. Voss, J.L. Osborn, Ion channel signaling influences cellular proliferation and phagocyte activity during axolotl tail regeneration, Mech. Dev. 146 (2017) 42–54, https://doi.org/10.1016/j.mod.2017.06.001.
[78] P. Valverde, T. Kawai, M.A. Taubman, Selective blockade of voltage-gated potassium channels reduces inflammatory bone resorption in experimental periodontal disease, J. Bone Miner. Res. 19 (2003) 155–164, https://doi.org/10.1359/jbmr.0301213.
[79] S.J. Petty, C.J. Milligan, M. Todaro, K.L. Richards, P.K. Kularathna, C.N. Pagel, C.R. French, E.L. Hill-Yardin, T.J. O'Brien, J.D. Wark, E.J. Mackie, S. Petrou, The antiepileptic medications carbamazepine and phenytoin inhibit native sodium currents in murine osteoblasts, Epilepsia. 57 (2016) 1398–1405, https://doi.org/10.1111/epi.13474.
[80] R.B. Moraes, L. Corrêa, J.G.C. Luz, Adverse effects of the amlodipine on bone healing of the mandibular fracture: an experimental study in rats, Oral Maxillofac. Surg. 15 (2011) 93–101, https://doi.org/10.1007/s10006-010-0237-6.
[81] Y. Atalay, F. Bozkurt, Y. Gonul, O. Cakmak, K.S. Agacayak, I. Kose, O. Hazman, H. Keles, O. Turamanlar, M. Eroglu, The effects of amlodipine and platelet rich plasma on bone healing in rats, Drug Des. Devel. Ther. (2015) 1973, https://doi.org/10.2147/DDDT.S80778.
[82] B.A. Brouwer, I.S.J. Merkies, M.M. Gerrits, S.G. Waxman, J.G.J. Hoeijmakers, C.G. Faber, Painful neuropathies: the emerging role of sodium channelopathies, J. Peripher. Nerv. Syst. 19 (2014) 53–65, https://doi.org/10.1111/jns5.12071.
[83] J. Park, Z.D. Luo, Calcium channel functions in pain processing, Channels (Austin) 4 (2010) 510–517.
[84] C. Tsantoulas, S.B. McMahon, Opening paths to novel analgesics: the role of potassium channels in chronic pain, Trends Neurosci. 37 (2014) 146–158, https://doi.org/10.1016/j.tins.2013.12.002.
[85] C. Tsantoulas, L. Zhu, P. Yip, J. Grist, G.J. Michael, S.B. McMahon, Kv2 dysfunction after peripheral axotomy enhances sensory neuron responsiveness to sustained input, Exp. Neurol. 251 (2014) 115–126, https://doi.org/10.1016/j.expneurol.2013.11.011.
[86] L.-Y. Chien, J.-K. Cheng, D. Chu, C.-F. Cheng, M.-L. Tsaur, Reduced expression of A-type potassium channels in primary sensory neurons induces mechanical hypersensitivity, J. Neurosci. 27 (2007) 9855–9865, https://doi.org/10.1523/JNEUROSCI.0604-07.2007.